analysis of the relationship between intracellular Ca^{2+} concentration and neurotransmitter release. However, in their work, the electrochemical and fluorescent images of PC12 were captured in constant-height mode. The current profiles in the electrochemical image only reflected the topography of the neuron without providing any information on chemical characteristics.

Shear force distance regulation has enabled the successful imaging of living cellular surfaces with near-field scanning optical microscopy (NSOM),[29−31] but SECM imaging is still difficult because the apexes of SECM electrodes are generally larger than NSOM fiber probes. We successfully imaged single-cell topography and respiration activity using a conical-shaped optical fiber electrode.[17] However, the sensitivity of conical-shaped electrodes is low because the ratio of the electrode surface area near the cellular surface is very small.[32] To circumvent this problem, the apex of the probe should be made of disk- or ring-shaped electrodes. In this study, we employed a focused ion beam (FIB) to mill the probe apex and form ring electrodes. FIB allows the milling of a specific region selectively under FIB observation.

For successful imaging of living cell topography with scanning force microscopy, the magnitude of force interaction between the probe and cell should, in general, be less than 30 nN.[33] Although several studies reported theoretical approaches to detect shear force using a tuning fork,[34,35] most of them involved the calculation of forces in an air state, which was apparently unsuitable for performing measurements of living cells. In this study, we optimized the operating conditions of the vibrating probe to detect shear forces against living cells when the probe approaches at different oscillation amplitudes.

The probe scanning program also plays an important role in the imaging of living cell topography. The standing approach (STA) mode, in which the probe repetitively approaches the sample surface and retracts at each point, is a promising method for imaging the convoluted surface topography of living cells.[17,20] Similar scanning methods were reported by other groups.[18,36] However, such image acquisition takes too much time as compared to conventional lateral scanning methods. To resolve this problem, Korchev et al. changed the step size during measurement by prescanning the scan area.[37] In our system, we improved the feedback regulation speed by incorporating field-programmable gate arrays (FPGAs).

In this study, the inner and outer functions of single living cells were evaluated using an optical fiber-nanoelectrode probe with a shear force feedback system (Figure 1). This probe enables us to detect and induce electrochemical and photochemical reactions simultaneously. Smyrl et al. reported a photochemical study that used an SECM/optical microscope (OM) to realize a laser-induced photochemical reaction using an optical fiber and detect the reaction using a ring electrode.[38,39] In the present report, HeLa cells, transfected with two expression vectors including secreted alkaline phosphatase (SEAP) and green fluorescent protein (GFP), were used to demonstrate simultaneous topographic, electrochemical, and fluorescent imaging of living cells. SEAP has a unique feature that is secreted from the cell. Extracellular SEAP can be electrochemically detected by using *p*-aminophenylphosphate (PAPP) as a substrate.

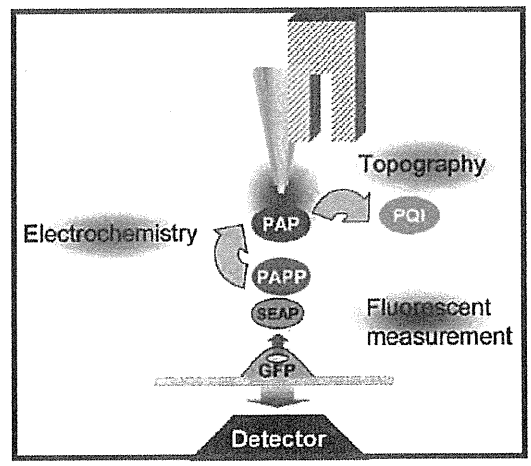

Figure 1. Schematic representation of simultaneous topographic, electrochemical, and optical imaging of a single transfected cell. Secreted alkaline phosphatase (SEAP) and green fluorescence protein (GFP) were cotransfected in HeLa cells.

EXPERIMENTAL SECTION

Chemicals. *p*-Aminophenylphosphate monosodium salt (PAPP; LKT Laboratory Inc.) and ferrocenemethanol (FcMetOH; Aldrich) were purchased and used as received (as were all the other chemicals used in this study). All the solutions were prepared using distilled water obtained from a Milli-Q ultrapure water purification system (Millipore, Japan).

Cell Culture and Transfection. HeLa cells obtained from a human cervix epithelial cell line were cultured in Petri dishes (Falcon) with RPMI1640 medium (Gibco) containing 10% fetal bovine serum (FBS; Gibco), 50 μg mL^{-1} penicillin, and 50 μgmL^{-1} streptomicyne in a humidified incubator (37 °C in an atmosphere of 5% CO_2). The cells were trypsinized in a 0.25% trypsin solution and seeded (3×10^5 cells mL^{-1}) onto culture plates such as protein-patterned substrates. HeLa cells were transfected with a GFP vector (pAcGFP1-N1, 4.7 kb, BD Sciences) or cotransfected with the GFP vector and pSEAP2-control vector (5.1 kb, BD Sciences). The cells were seeded in a 35-mm dish (Falcon) at a density of 5×10^5 cells in 2 mL of RPMI-1640 medium containing 10% FBS without antibiotics. After cultivation for 1 day, transfection was performed by the

(29) Koopman, M.; Cambi, A.; de Bakker, B. I.; Joosten, B.; Figdor, C. G.; van Hulst, N. F.; Garcia-Parajo, M. F. *FEBS Lett.* 2004, *573*, 6–10.
(30) de Bakker, B. I.; de Lange, F.; Cambi, A.; Korterik, J. P.; van Dijk, E. M.; van Hulst, N. F.; Figdor, C. G.; Garcia-Parajo, M. F. *ChemPhysChem.* 2007, *8*, 1473–1480.
(31) de Bakker, B. I.; Bodnar, A.; van Dijk, E. M.; Vamosi, G.; Damjanovich, S.; Waldmann, T. A.; van Hulst, N. F.; Jenei, A.; Garcia-Parajo, M. F. *J. Cell Sci.* 2008, *121*, 627–633.
(32) Mirkin, M. V.; Fan, F. R. F.; Bard, A. J. *J. Electroanal. Chem.* 1992, *328*, 47–62.
(33) Henderson, E.; Haydon, P. G.; Sakaguchi, D. S. *Science* 1992, *257*, 1944–1946.
(34) Karrai, K.; Grober, R. D. *Appl. Phys. Lett.* 1995, *66*, 1842–1844.
(35) Karrai, K.; Grober, R. D. *Ultramicroscopy* 1995, *61*, 197–205.
(36) Borgwarth, K.; Ebling, D. G.; Heinze, J. *J. Ber. Bunsen-Ges. Phys. Chem.* 1994, *98*, 1317–1321.
(37) Novak, P.; Li, C.; Shevchuk, A. I.; Stepanyan, R.; Caldwell, M.; Hughes, S.; Smart, T. G.; Gorelik, J.; Ostanin, V. P.; Lab, M. J.; Moss, G. W.; Frolenkov, G. I.; Klenerman, D.; Korchev, Y. E. *Nat. Methods* 2009, *6*, 279–281.
(38) James, P. I.; Garfias-Mesias, L. F.; Moyer, P. J.; Smyrl, W. H. *J. Electrochem. Soc.* 1998, *145*, L64–L66.
(39) James, P.; Casillas, N.; Smyrl, W. H. *J. Electrochem. Soc.* 1996, *143*, 3853–3865.

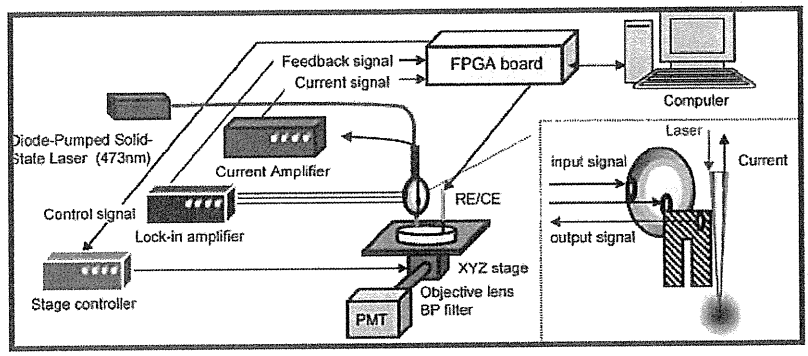

Figure 2. Schematic diagram of the SECM/OM system with shear force feedback regulation.

addition of 500 μL of Opti-MEM I medium (Gibco) containing 4 μg of plasmid DNA and 10 μL of Lipofect AMINE 2000 (Invitrogen). The cells were then incubated at 37 °C overnight.

Measurement System. The configuration of the SECM/OM system with feedback control of probe-sample distance was basically the same as that reported previously.[17] A FPGA board (NI-7831R, National Instruments) was incorporated into the basic system to improve the speed of feedback regulation. A schematic diagram is shown in Figure 2. FPGA is a device that contains a matrix of reconfigurable gate array logic circuitry. It is capable of executing complex discrete signal processing algorithms with clock rates of 40 MHz at maximum. Probe-sample distance feedback control and data acquisition were achieved without compromising the performance of the main PC operation.

For topography measurement, the probe was attached to one of the prongs of a tuning fork and vibrated using a piezoelectric buzzer (0.5−1 mV p−p, sine wave) to drive the tuning fork into the resonance state. The resonance frequency of the unprocessed tuning fork was 32 768 (2^{15}) Hz. The vibration signal from tuning fork was detected by a lock-in amplifier. The output time constant of the lock-in amplifier was set 3 ms. To synchronize the lock-in amplifier output signal with FPGA, the 3 ms signal from lock in amplifier was summed and leveled on FPGA.

Probe Scanning Program. We used the STA mode, which involves repetitive steps of approach toward the surface and retraction of the tip at each measurement point.[20,40] First, the probe position was set far from the sample, and the original tuning fork amplitude at a resonance frequency was measured (3 ms). The probe approached the sample until the tuning fork signal amplitude reduced to 1% of the original signal. The signal reduction is caused by the shear force between the probe tip and the sample surface. The approach process takes about 50−100 ms. The speed and accuracy of this process was enhanced dramatically by adopting the FPGA board. Next, the probe was lifted by 50 nm to acquire the current/optical signal for 100 ms. Vertical movement of the probe may be caused by liquid convection. Therefore, we waited 10 ms before recording the current/optical signal. The probe was further raised by about 0.1−3.0 μm to avoid contacting the sample surface. By repeating these processes at every measurement point, the probe can follow the changing shape of the sample and maintain a constant distance to sample as noncontact.

Fabrication of an Optical Fiber Electrode. A single-mode optical fiber (New Port, F-SA) was pulled using a carbon dioxide laser puller (Sutter Instruments, Model P-2000). The fiber was then coated with a Ti/Pt layer by sputtering (Anelva, L-332S-FH, RF200) and subsequently insulated with a xylene polymer (parylene C, Daisan Kasei) via vapor deposition polymerization (PDS-2010, Parylene Japan). To expose an electroactive area and form an optical aperture, the probe apex was milled by a focused ion beam (FIB, Seiko Instruments, SMI 2050).

Measurement Methods of SEAP and GFP. SEAP catalyzes the hydrolysis of PAPP to produce *p*-aminophenol (PAP), which is oxidized at a tip electrode potential of 0.3 V vs Ag/AgCl. The electrochemical detection of PAP allows the continuous quantification of SEAP expression in the genetically engineered cell. Concurrent with the electrochemical measurements, a laser light (wavelength = 473 nm) was introduced to excite GFP expressing inside the cell. Light emitted from the sample was collected by a photomultiplier tube (PMT, Hamamatsu H5920-01) through a long-pass filter (>520 nm) to obtain a fluorescent image.

RESULTS AND DISCUSSIONS

To realize electrochemical and fluorescent detection of gene expression at the single-cell level, we tried to improve the sensitivity of the SECM/OM. First, we fabricated an optical fiber-nanoelectrode probe, which could simultaneously detect chemical information from the cellular surface and optical information from inside the cell. Second, the amplitude of tuning fork oscillation was optimized for shear-force-based distance regulation to trace the surface of the living cell. Third, improvement concerning the feedback speed for distance regulation by incorporating an FPGA board.

Characterization of Optical Fiber Electrode. Figure 3a shows a scanning electron microscopy (SEM) image of the optical fiber- nanoelectrode probe. The radii of the inner and outer rings of the electrode and the insulator layer were 37, 112, and 320 nm, respectively. Figure 3b shows the cyclic voltammogram (CV) of this electrode in 0.5 mM FcMetOH and 0.1 M KCl at a scanning rate of 20 mV/s. The steady state current (150 pA) was larger than that calculated for a 112 nm-radius disk electrode (16 pA). As the ratio of the outer-to-inner ring radius was much larger than 1.25, the edge effect peculiar to the ring electrode could not be seen; thus, the CV behavior of the ring electrode was almost the same as that of the disk electrode.[41] Figure 3c shows the tip current profile as a function of the tip−sample distance when the

(40) Takahashi, Y.; Miyamoto, T.; Shiku, H.; Asano, R.; Yasukawa, T.; Kumagai, I.; Matsue, T. *Anal. Chem.* 2009, *81*, 2785–2790.

(41) Lee, Y.; Amemiya, S.; Bard, A. *J. Anal. Chem.* 2001, *73*, 2261–2267.

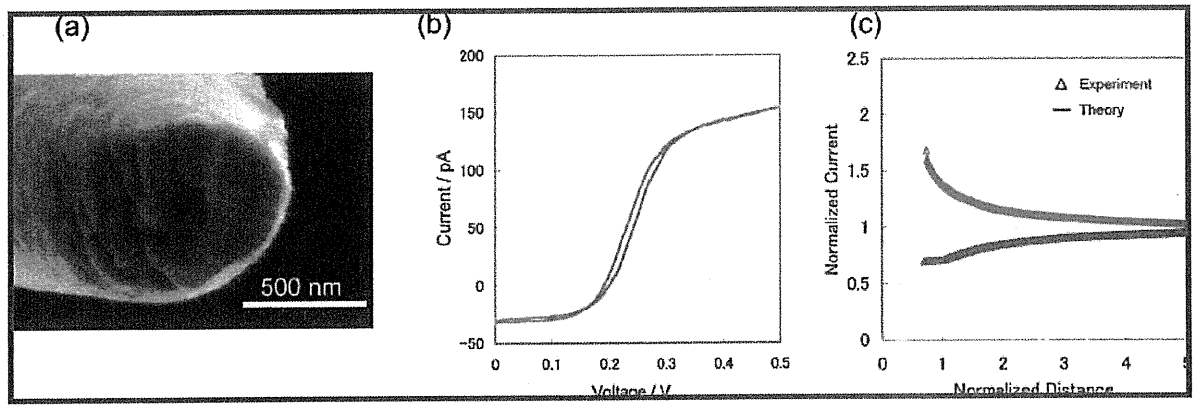

Figure 3. Characteristics of an optical fiber electrode. (a) Scanning electron microscopy micrograph. (b) Cyclic voltammogram of an optical fiber electrode probe in 0.5 mM ferrocenemethanol(FcMetOH) and 0.1 M KCl at a scan rate of 20 mV/s. (c) Approach curve of normalized current for Pt and glass substrates was plotted at a probe potential of +0.50 V (vs Ag/AgCl) in 0.5 mM FcMetOH and 0.1 M KCl. The tip−sample distance was normalized to the tip radius of 785 nm.

tip approaches the glass substrate. In this experiment, we used a 785 nm-radius electrode. This electrode steady state current (240 pA) was also larger than the theoretical one (112 pA). There is a possibility that the defects in the insulating layer at the side of the electrode caused larger current, although the defect of insulating layer was not able to observe using SEM. The smaller electrode (112 nm-radius, Figure 3b) tended to present a larger deviation in currents between the theoretically estimated from SEM image and the experimentally observed with amperometry than the larger electrode (785 nm-radius, Figure 3c).

In spite of a disagreement of the steady state current, both conductive and nonconductive samples demonstrated clearly visible feedback effects in their respective approach curves. The experimental curves were well fitted with the theoretical curves plotted with the assumption of RG 2.0 (RG, dimensionless insulator radius of the tip normal to the electrode radius of the tip).[42] Although several groups have reported the fabrication of nanoelectrodes, few researchers have obtained approach curves that provide current changes because of positive or negative feedback at a tip−sample distance smaller than the tip radius. For probe electrodes of conical or hemispherical shape, feedback effects are not clearly visible. We tried to flatten the probe apex by milling with FIB to improve current sensitivity and spatial resolution. The FIB process increased the success rate of fabrication of the optical fiber-ring nanoelectrode probe by >90%. This electrode is suitable to detect cellular chemical properties.

Optimization of the Shear Force during Tip−Sample Distance Regulation. In shear force distance regulation, the amplitude of the tuning fork to which the probe is attached is the most important parameter for living cellular topography imaging. Damage to the cell increases when the tuning fork amplitude becomes larger. Therefore, the amplitude must be small enough to minimize the damage to the fragile cellular surface. However, when the amplitude was set at a very small value, the force caused by the solution viscosity interfered with the shear force detection. We investigated the correlation between the amplitude and the sensitivity of the tuning fork by using a glass capillary probe. As a sample, HeLa cells cultured in a 35-mm Petri dish filled with 2 mL RPMI medium were used. Figure 4a shows the approach curves obtained when the probe approaches the living cell surface at tuning fork amplitudes of 1 mV, 100 μV, or 10 μV. The tuning fork amplitude was normalized to the tuning fork amplitude of free oscillation in solution. When the probe approached the cell, the tuning fork amplitude reduced at the cell membrane surface ($z = 8$ μm) and also significantly decreased at the bottom of the culture dish ($z = 1$ μm). Importantly, when the tuning fork amplitude was set at 1 mV, the probe could not sense the cellular surface because the oscillation force was too strong to perform cell-surface measurements. When the turning fork amplitude was set at 10 μV, the force of solution viscosity interfered with the shear force detection and increased the noise level. Figure 4b shows topographies of HeLa living cells when the starting signal amplitudes of the tuning fork were adjusted to 30 μV and 75 μV. In shear-force-based distance regulation, the probe approached the surface until the tuning fork amplitude reduced to 1% of the original tuning fork amplitude. A clear image could be acquired when the tuning fork amplitude was set at 75 μV. Random noises were evident in the image obtained at the amplitude of 30 μV. When the tuning fork amplitude was set at 150 μV, the topography could not be imaged (not shown). Therefore, the starting tuning fork amplitude was adjusted to about 70−80 μV for imaging living cells. The optimal tuning fork amplitude depends on the design of the distance regulation probe, the shape of the probe, and the depth of the probe in the solution. Therefore, we carried out all experiments under the same conditions.

Improvement of Feedback Speed during Distance Regulation. Figure 5 shows the topography images of living HeLa cells observed using the shear force distance regulation system. Because of rapid FPGA data processing, the time required for imaging was drastically reduced when compared with the imaging time in the previous system without FPGA processing. Figure 5a shows the topography image of living mammalian cells in the range of 100 × 100 μm^2 with 1-μm stepsize (or 10 000 data points). The acquisition of shear-force signals to image the topography was completed within 30 min; thus, a 12-fold decrease in acquisition time was achieved as compared to the previous system. Moreover, higher resolution imaging can be

(42) Shao, Y. H.; Mirkin, M. V. *J. Phys. Chem. B* **1998**, *102*, 9915–9921.

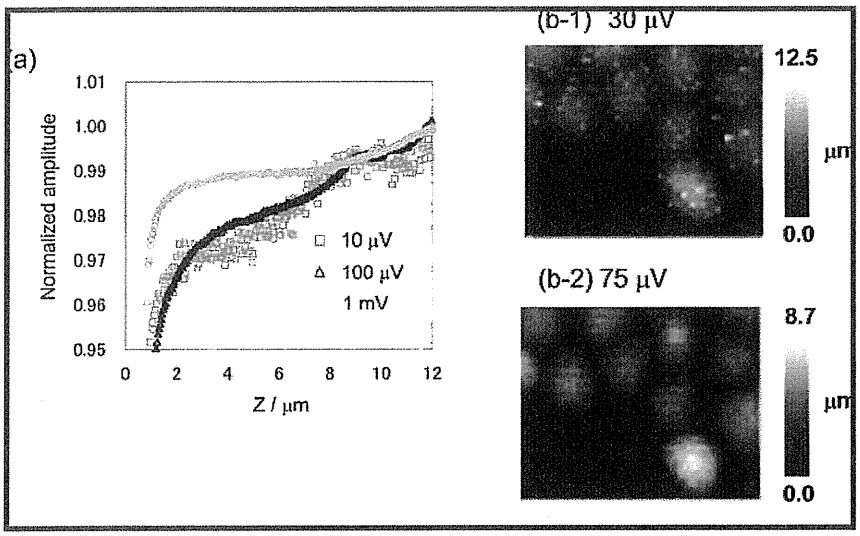

Figure 4. Optimization of tuning-fork amplitude for living cell topography imaging. (a) Tuning for amplitude-distance profiles of a living cellular surface. (b) Topography images of HeLa cells at tuning fork amplitudes of 30 μV and 75 μV. The scan range was 100 μm × 80 μm, and the step size was 2.0 μm.

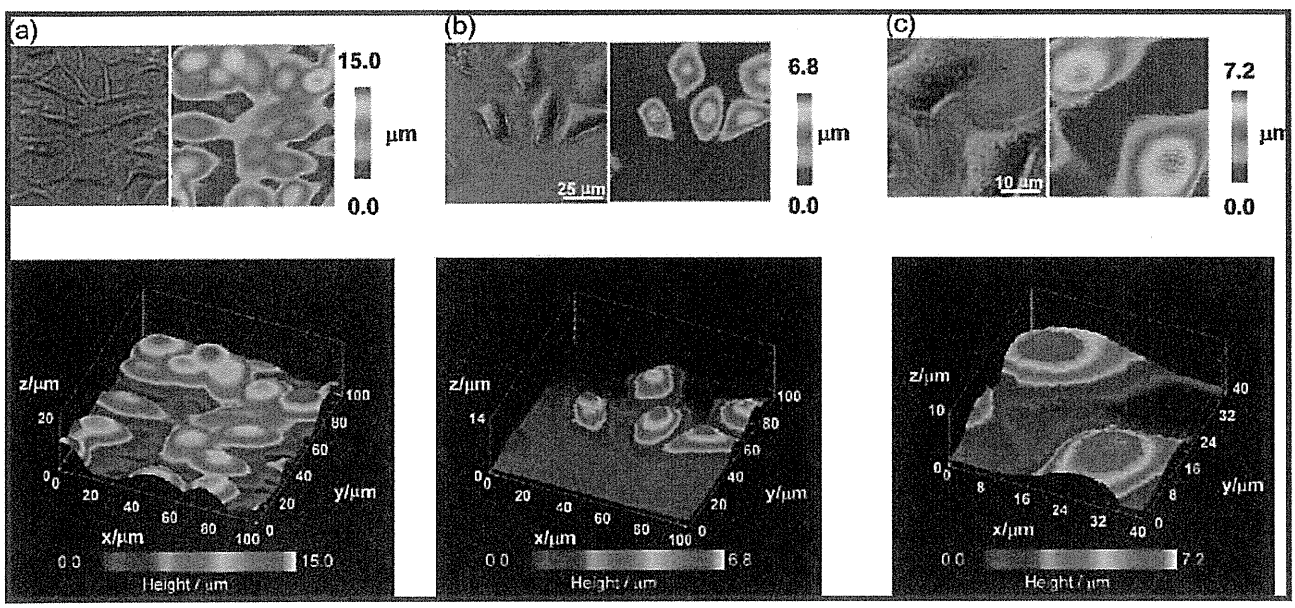

Figure 5. Optical micrograph and two- and three-dimensional topographically rendered images of (a) MCF-7 cells and (b, c) HeLa cells in a culture medium RPMI-1640 in the standing approach (STA) mode using a capillary probe. The respective scan ranges and step sizes were (a) 100 μm × 100 and 1.0 μm, (b) 100 μm × 100 and 0.5 μm, and (c) 40 μm × 40 and 0.2 μm.

realized because of the shorter imaging time. Figure 5b and c shows topography images with 0.5 and 0.2 μm stepsize, respectively. The clear cellular surface topography images indicated that the maximum cellular height was approximately 7 μm.

GFP-Expressed HeLa Cell Images. The expression of GFP in HeLa cells was measured in RPMI-1640 medium in constant-distance and constant-height modes. In the constant-height mode, the probe was positioned 10 μm above the sample surface to prevent the probe tip from making contact with the sample surface during the scanning process. Figure 6 shows topographic and fluorescent images of HeLa cells. The cell topography conforms extremely well to the OM images of the cell. On the basis of the topography, the height of the HeLa cells was estimated to be 6.5 μm. It should also be noted that the fluorescent images obtained in the constant-distance mode (Figure 6c-1) were much sharper than those obtained in the constant-height mode (Figure 6c-2). The superiority of constant-distance imaging over constant-height imaging is evident in the cross-sectional fluorescence signals (Figure 7) at the lines indicated in Figure 6c. The half widths of the fluorescent peaks are found to be 18 μm for the constant-distance mode and 31 μm for the constant-height mode, indicating that distance regulation plays a crucial role in bioimaging based on fluorescence emission.

Since gene-expression levels in individual cells are influenced by intracellular processes such as transcription, translation, and postmodification, long-term monitoring of gene expression at the single-cell level is indispensable from the viewpoint of understanding intracellular signaling in greater detail. However, fluorescent

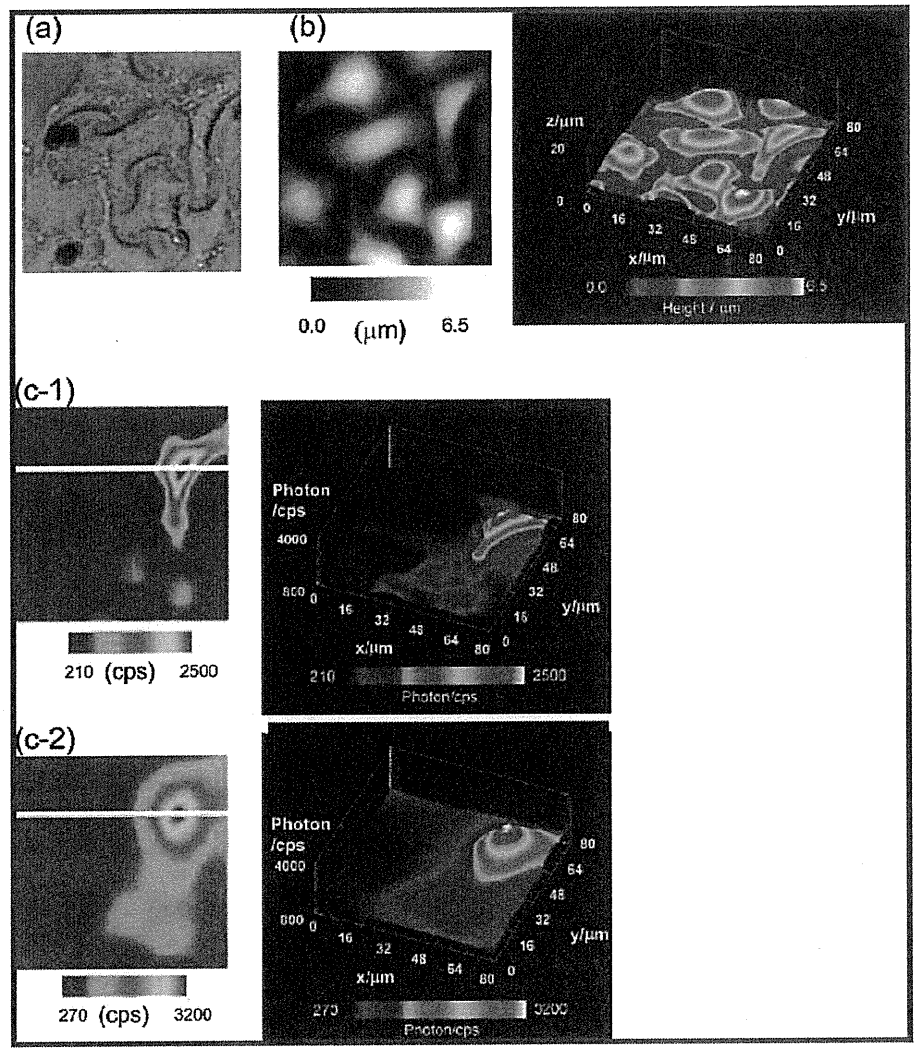

Figure 6. Optical (a), topographical (b), and two- and three-dimensional fluorescent (c) images of GFP-transfected HeLa cells. The topography image (b) was obtained by using shear force feedback distance modulation. Fluorescent images were obtained in the constant-distance mode (c-1) and constant-height mode (c-2). In the constant-height mode, the height was set at 10 μm above the substrate, and the scan rate was 3 μm/s. The scan range was 80 μm × 80 μm, and the step size was 1.0 μm.

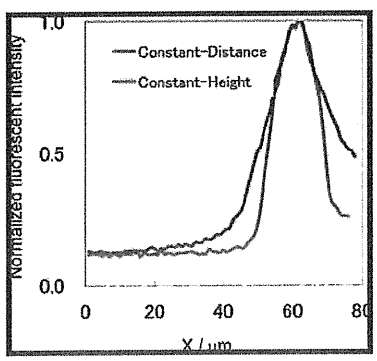

Figure 7. Cross-section of fluorescent signals of the image shown in Figure 6 in the constant-height and constant-distance modes. The fluorescent intensity was normalized with the maximum fluorescent intensity.

detection using a reporter protein such as GFP has serious drawbacks. First, it is unstable for long-term monitoring because excited light damages to the cell. Second, quantitative analysis is problematic because of photobleaching. Electrochemical detection of gene expression, on the other hand, can be improved by using microarray-based systems with long-term monitoring, fast detection, and high throughput.[43,44] Furthermore, an electrochemical reporter system can be combined with other optical instruments used in the cotransfection reporter assay to provide a novel assay protocol, making it easy for us to distinguish specific reporter proteins.

Simultaneous Detection of GFP and SEAP Coexpressed in a Single HeLa Cell. Lipofection realizes cotransfection with two different vectors and has widely been used for investigating transcription factors, adhesion molecules, transporters, and protein–protein interactions.[45,46] Generally, cotransfection requires different reporter proteins in order to prevent gene

(43) Torisawa, Y. S.; Ohara, N.; Nagamine, K.; Kasai, S.; Yasukawa, T.; Shiku, H.; Matsue, T. *Anal. Chem.* **2006**, *78*, 7625–7631.
(44) Lin, Z. Y.; Takahashi, Y.; Murata, T.; Takeda, M.; Ino, K.; Shiku, H.; Matsue, T. *Angew. Chem., Int. Ed.* **2009**, *48*, 2044–2046.
(45) Desai, M. A.; Burnett, J. P.; Mayne, N. G.; Schoepp, D. D. *Mol. Pharmacol.* **1995**, *48*, 648–657.
(46) Jones, F. S.; Prediger, E. A.; Bittner, D. A.; Derobertis, E. M.; Edelman, G. M. *Proc. Natl. Acad. Sci. U.S.A.* **1992**, *89*, 2086–2090.

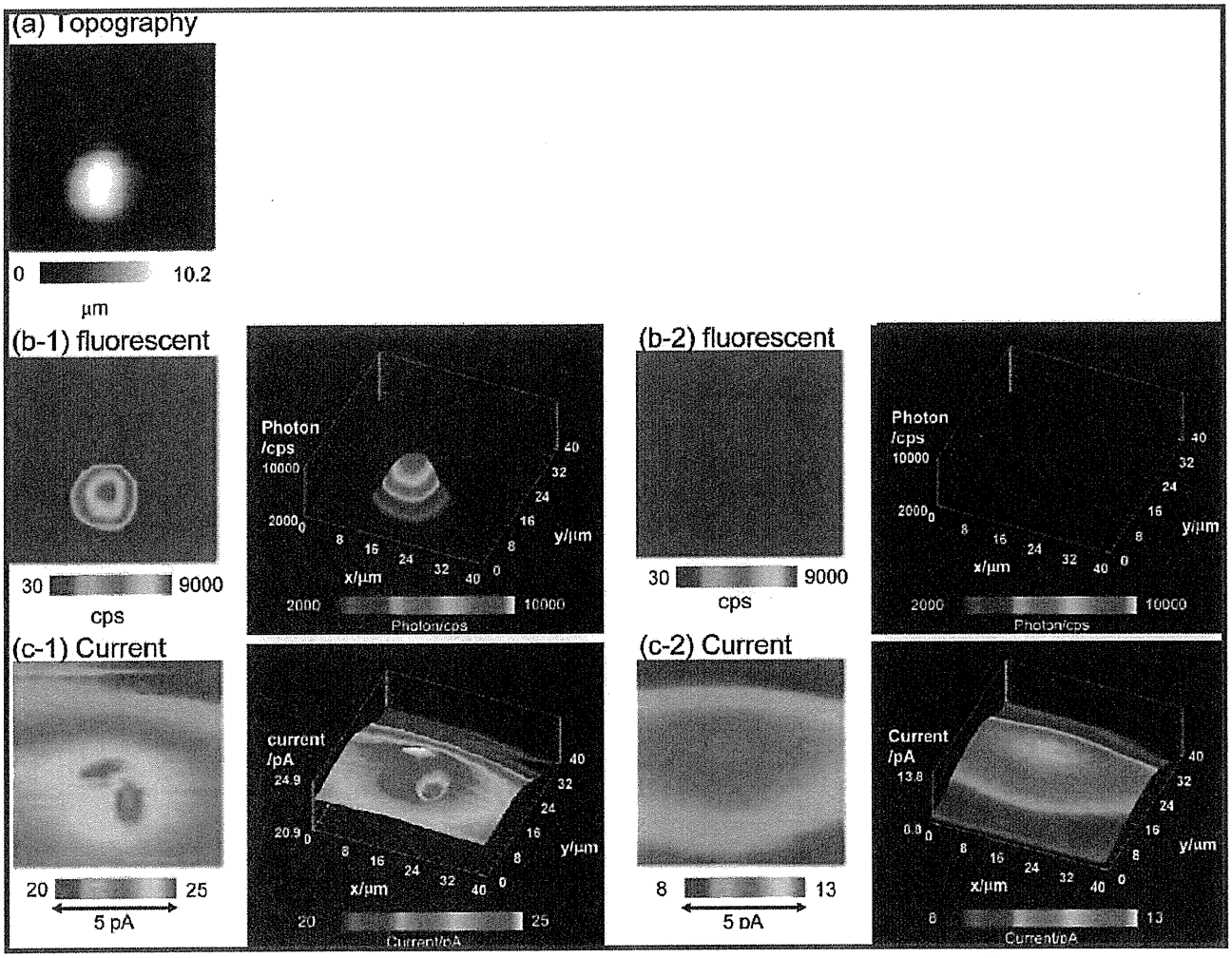

Figure 8. Simultaneous topographic (a), fluorescent (b-1 and b-2), and electrochemical (c-1 and c-2) images of a GFP- and SEAP-transfected single HeLa cell obtained in the constant-distance mode (a, b-1, and c-1) and constant-height mode (b-2 and c-2). In constant-height mode imaging, the height was set at 15 μm above the substrate, and the scan rate was 3 μm/s. The scan range was 40 μm $\times$ 40 μm, and the step size was 1.0 μm. The approximate inner and outer radii of the ring electrode were 200 and 480 nm, respectively.

expression from each vector. Although a set of fluorescence proteins with different colors has been employed to distinguish specific expressed proteins, there is a potential need to develop other detection methods for reporter proteins that are fundamentally different from fluorescent detection. Among other possible methods, electrochemical detection is a promising candidate. However, few reports have demonstrated that gene expression is electrochemically detectable at the single-cell level.[47] To our knowledge, the current study is the first to measure the gene expression of single cells based on fluorescence and electrochemistry.

Simultaneous topography, fluorescent, and electrochemical images of transfected single HeLa cells were obtained in constant-distance and constant-height modes (Figure 8). In the constant-height mode, the probe was positioned 15 μm above the sample surface and scanned in a HEPES-based saline solution (pH 9.5) containing 4.7 mM PAPP. When the probe moves above the HeLa cell, the intensity of the electrochemical signal increases as a result of the oxidation of PAPP generated by an enzyme reaction of SEAP. Two-dimensional acquisition of the electrochemical signals provides SECM images of cells with high enzyme-expression capabilities. The time required to image a 40 $\times$ 40 μm^2 area with 1-μm stepsize was typically 40 min. The constant-distance mode permits a higher contrast than the constant-height mode because the concentration of SEAP was high near the cell. Distance regulation is also important to improve electrochemical measurement sensitivity. The current response was found to decrease due to probe damping in the constant-distance mode when the probe approached the cell. Although we optimized our system for optical fiber electrode measurement, it was difficult to realize shear force distance regulation in the constant-distance mode because of the problems related to the structure of the probe and the solution in which measurements were carried out. For effective detection of shear force, we milled the probe at an angle of 60° to reduce the area of shear force interaction between the probe and the cell. Milling the probe to an angle of 90° resulted in interaction over a large area, due to which a clear signal corresponding to the shear force could not be obtained from the living cellular surface. In the present study, we used a HEPES-based saline solution with

(47) Chang, C. Y.; Takahashi, Y.; Murata, T.; Shiku, H.; Chang, H. C.; Matsue, T. *Lab Chip* 2009, *9*, 1185–1192.

pH 9.5, an optimum pH for SEAP. At this pH, the cellular membrane became unstable, although the cells remained alive for at least 3 h in the measuring solution. The membrane instability also gave rise to shear force instability and made constant-distance mode measurements impossible. Nevertheless, our study is the first to report simultaneous topographical, fluorescent, and electrochemical imaging of living cells with discrimination of the outer and inner cellular states.

CONCLUSION

In this study, we simultaneously measured two reporter proteins, SEAP secreted from the cell to an outside solution and GFP expressed inside the cell, by using an SECM/OM system. Furthermore, we combined the system with shear force distance regulation to simultaneously detect topography, improved electrochemical responses, and fluorescent signals at the single-cell level. Previously, we reported the imaging of membrane proteins of living cells by using SECM.[40] The combination of fluorescent and electrochemical measurements is particularly useful for analyzing the dynamics of cellular membrane proteins, because the electrochemical response changes dramatically when the membrane proteins move inside the cell. Future work will focus on membrane protein endocytosis by further developing the SECM/OM.

ACKNOWLEDGMENT

This work was partly supported by Grants-in-Aid for Scientific Research (18101006 and 21685008) from MEXT (Ministry of Education, Culture, Sports, Science, and Technology), Japan, by a Grant-in-Aid for Scientific Research on Priority Areas (17066002) "Life Surveyor" from MEXT, and by a grant from the Center for Interdisciplinary Research, Tohoku University. Y.T. also acknowledges the support obtained from a research fellowship of the Japan Society for the Promotion of Science.

SUPPORTING INFORMATION AVAILABLE

Characterization of tuning fork, amplitude and phase images of GFP- and SEAP-transfected single and simultaneous topographic, fluorescent, and electrochemical images of a GFP- and basic-SEAP-transfected single HeLa cell. This material is available free of charge via the Internet at http://pubs.acs.org.

Received for review August 9, 2009. Accepted October 10, 2009.

AC901796R

Biosensors and Bioelectronics 25 (2009) 913–919

Contents lists available at ScienceDirect

Biosensors and Bioelectronics

journal homepage: www.elsevier.com/locate/bios

Electrochemical single-cell gene-expression assay combining dielectrophoretic manipulation with secreted alkaline phosphatase reporter system

Tatsuya Murata[a], Tomoyuki Yasukawa[b], Hitoshi Shiku[a,*], Tomokazu Matsue[a,**]

[a] Graduate School of Environmental Studies, Tohoku University, Aramaki Aoba 6-6-11, Sendai 980-8579, Japan
[b] Graduate School of Material Science, University of Hyogo, 3-2-1 Kouto, Kamigori-cho, Ako-gun, Hyogo 678-1297, Japan

ARTICLE INFO

Article history:
Received 9 July 2009
Received in revised form 20 August 2009
Accepted 1 September 2009
Available online 6 September 2009

Keywords:
Scanning electrochemical microscopy
Single-cell analysis
Reporter
Dielectrophoresis

ABSTRACT

Scanning electrochemical microscopy (SECM) was used for the analysis of single-cell gene-expression signals on the basis of a reporter system. We microfabricated a single-cell array on an Indium tin oxide (ITO) electrode comprising 4 × 4 SU-8 microwells with a diameter of 30 μm and a depth of 25 μm. HeLa cells transfected with plasmid vectors encoding the secreted alkaline phosphatase (SEAP) were seeded in the microwell at a concentration of 1 cell per well by positive-dielectrophoresis (pDEP). A pDEP pulse of 3.0 Vpp and 1 MHz was applied between the microwell array/ITO electrode and an ITO counter electrode located on the top of the flow-cell assembly of the microdevice. The electrochemical responses of the individual HeLa cells transfected with SEAP were significantly larger than those of the wild-type HeLa cells. The electrochemical response of the transfected single cells was statistically distinguishable from that of wild-type HeLa cells. The size of the wells and the material of the single-cell array were optimized in order to evaluate the tumor necrosis factor α (TNF-α)-induced activation process of nuclear factor kappa B (NFκB) that was used as the model for on-chip monitoring of cellular signal transduction.

1. Introduction

The living cell is itself an integrated sensing system by which highly sophisticated functional operation and parallel signal transduction pathways are systematically processed. Receptor proteins on the cell membrane or in the cytoplasm interact with specific ligand molecules, and consequently, this ligand-receptor binding induces conformational changes in proteins or in the molecular assembly. Reporter assay is frequently used in gene-expression studies; it involves incorporation of a vector plasmid carrying a reporter gene into the cells or the fusion of a promoter with the reporter gene. In a whole-cell reporter system, an analyte binds to a regulatory protein inducing reporter gene expression. Consequently, the reporter protein generates a detectable signal that can be measured by techniques such as photometry, radiometry, fluorescence, or colorimetry (Daunert et al., 2000). We selected alkaline phosphatase, which catalyzes the hydrolysis of phosphoric group, as the reporter enzyme (Kelso et al., 2000; Torisawa et al., 2006; Neugebauer et al., 2009). Secreted alkaline phosphatase (SEAP) hydrolyzes *p*-aminophenylphosphate (PAPP) to *p*-aminophenol (PAP), which is an electrochemically active species. On these lines, we attempted to construct an electrochemical detection system by using microelectrode scanning technique (Torisawa et al., 2006; Shiku et al., 2009) and an electrochemical device (Lin et al., 2008, 2009; Yasukawa et al., 2008). In the present study, single-cell imaging of HeLa cells transfected with SEAP was performed by scanning electrochemical microscopy (SECM) (Bard et al., 1989; Mauzeroll and Bard, 2004; Bard et al., 2006; Li and Bard, 2009; Wittstock et al., 2007; Roberts et al., 2007; Takahashi et al., 2006, 2009) and compared with the concurrent responses of the wild-type HeLa cells.

Miniaturized well array and microfluidics have been shown to improve the throughput, sensitivity, and cost performance of single-cell analysis (Sims and Allbritton, 2007). Various techniques have been applied for constructing single-cell arrays (Whitaker and Walt, 2007; Retting and Folch, 2005; Ino et al., 2008; Matsunaga et al., 2008; Hosokawa et al., 2009; Sasuga et al., 2008; Yamamura et al., 2005; Skelley et al., 2009; Kovac and Voldman, 2007; Di Carlo et al., 2006). In the present study, we used positive-dielectrophoresis (pDEP) (Matsue et al., 1993, 1997; Matsumoto et al., 1994; Lee et al., 2008, 2009; Kunikata et al., 2009) for single-cell manipulation. It is generally believed that single-cell manipulation by DEP preserves the viability of the cells and their normal functions (Suzuki et al., 2008; Gray et al., 2004; Kaff and Voldman, 2005). Using statistical analysis, we have successfully distinguished the electrochemical response of the transfected single cells from that of wild-type HeLa cells. Signal transduction was also examined using single-cell array, where tumor necrosis factor α (TNF-α)-induced activation of the

* Corresponding author. Fax: +81 22 795 6167.
** Corresponding author.
E-mail addresses: shiku@bioinfo.che.tohoku.ac.jp (H. Shiku), matsue@bioinfo.che.tohoku.ac.jp (T. Matsue).

0956-5663/$ – see front matter © 2009 Elsevier B.V. All rights reserved.
doi:10.1016/j.bios.2009.09.001

nuclear factor kappa B (NFκB) pathway was the model pathway for single-cell array analysis. The optimum material for the construction of the single-cell chamber array was determined. Our findings indicate that accurate analysis of signal transduction may be hindered by DEP manipulation and the SU-8 as material for the construction of the array, both of which may cause elevation in the background level of SEAP expression before TNF-α stimulation.

2. Experimental

2.1. Chemicals and materials

p-Aminophenol (PAP; Wako Pure Chemical Industries), 3,3,4,4,5,5,6,6,6-nonafluorohexyl trichlorosilane (LS-912; Shin-Etsu Chemical Co. Ltd.), 2-[4-(2-hydroxyethyl)-1-piperazinyl] ethanesulfonic acid (HEPES; Dojindo Laboratories, Japan), SU-8 (Microchem), SU-8 developer (Microchem), SU-8 sheet (XP film TRIAL-25; KAYAKU MICROCHEM Co. Ltd., Japan), poly(dimethylsiloxane) (PDMS; Silpot 184W/C, Dow Corning, USA), tumor necrosis factor-α (TNF-α; Wako Pure Chemical Industries), RPMI-1640 (Gibco Invitrogen, Tokyo, Japan), fetal bovine serum (FBS; Gibco), penicillin/streptomycin (Gibco), phosphate buffered saline (PBS(−); Wako Pure Chemical Industries), calcein-acetoxymethyl ester (calcein-AM; Dojindo Laboratories), propidium iodide (PI; Dojindo Laboratories), Opti-MEM I medium (Gibco), Lipofectamine™ 2000 (Invitrogen), and other chemicals were used as received. SEAP control vector (pSEAP2-Control) and the pNFκB-SEAP plasmid vector, in which a transfer element binding the κB site of the NFκB was located upstream of the *SEAP* reporter gene, were purchased from Clontech, BD Sciences. Indium tin oxide (ITO) electrode (4.50–4.98 Ω/sq) was purchased from Sanyo Vacuum Industries Co., Ltd. *p*-Aminophenylphosphate monosodium salt (PAPP) was purchased from LKT Lab Inc. or donated by Prof. Uichi Akiba from Akita University.

2.2. Cell culture and transfection

HeLa cells were donated by the Cell Resource Center for Biomedical Research (Tohoku University). The cells were cultured in RPMI-1640 containing 10% FBS and 50 μg mL^{-1} penicillin/streptomycin at 37 °C under a 5% CO_2 humidified atmosphere. The cultured HeLa cells were seeded in a 35-mm dish (Falcon) at a density of 5×10^5 cells in 2 mL of antibiotic-free RPMI-1640 medium containing 10% FBS. On the subsequent day, the cells were transfected with 500 μL of Opti-MEM I medium containing 4 μg of plasmid DNA and 10 μL of Lipofectamine™ 2000 and incubated for a further 5 h. Subsequently, the transfection medium was replaced by a fresh culture medium and the cells were incubated overnight at 37 °C.

2.3. Fabrication of single-cell array

We fabricated 3 types of array chips: microwell array/ITO, PDMS microwell array, and PDMS microstencil/polystyrene. The microwell array/ITO chip was designed to allow single-cell manipulation by pDEP). The microwell array/ITO chip with 6×4 or 6×6 arrays of cylindrical SU-8 microwell chambers was microfabricated on an ITO electrode. Each SU-8 microwell array (depth, 15 or 25 μm; diameter, 20, 30, 50 or 100 μm; gap between wells, 100 μm) was photolithographically patterned onto the ITO electrode as follows: the ITO electrode was either spin-coated with SU-8 or pasted with a SU-8 sheet at 50 °C and subsequently prebaked on a hotplate at 95 °C for 5 min. Then, the SU-8 layer was exposed to UV light for 30 s using a mask aligner, and the SU-8 coating was removed by using an SU-8 developer. The SU-8 microwell array/ITO chip was assembled with a 30 μm-thick poly(ethylene terephthalate) (PET) spacer and an ITO electrode on the top to construct a flow-through device (Fig. 1a). In order to pattern the cells with pDEP, the cells were suspended in a 0.2 M sucrose solution and injected into the device (Fig. 1a). pDEP manipulation was performed by applying an alternate current (AC) voltage (3 Vpp, 1 MHz) to the SU-8 microwell array/ITO chip and the top ITO electrode, in phase opposition so that the charge on each electrode is opposed at all times allowing the cells to deposit selectively in the microwells (Fig. 1b). After the wells were completely filled with cells, the current was turned off, and the cells outside the wells were removed by a slow-flowing stream of the medium (Fig. 1c). After disassembling the device, the

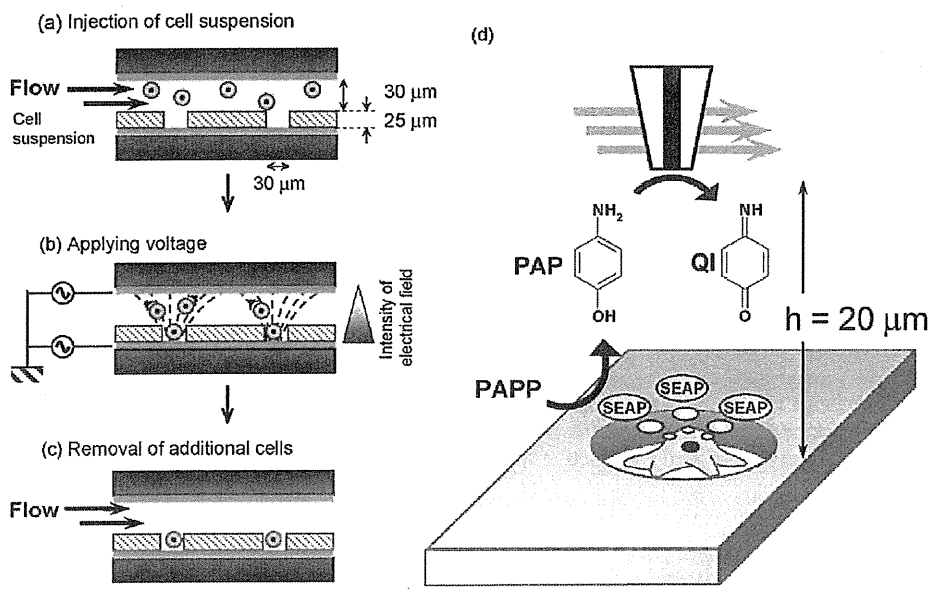

Fig. 1. Characterization of a reporter system using a single-cell array and electrochemical device. (a–c) Cell manipulation by pDEP; (d) the expression of the reporter enzyme SEAP is monitored electrochemically. PAPP was enzymatically hydrolyzed to produce PAP which was oxidized at +0.3 V vs. Ag/AgCl with the probe microelectrode. QI represents the product of electrooxidation. The height (*h*) of the electrode tip in the constant-height mode SECM was set at 20 μm from the top of the SU-8 or PDMS microwells.

cells in the microwell were incubated with the medium at 37 °C under 5% CO_2 for 5–7 h.

The PDMS microwell array without the ITO electrode was prepared by the same method as mentioned above and fabricated by using a SU-8 master on a silicon wafer. The SU-8 master was first treated with a silane coupling agent (LS-912) to prevent PDMS from adhering to the master. Next, the PDMS prepolymer was poured on the SU-8 master and cured in the oven at 80 °C for 2 h. After curing, the PDMS replica was removed from the SU-8 master and treated with O_2 plasma in an asher. The resultant replica was used as the PDMS microwell array. The PDMS microstencil/polystyrene chip was fabricated by placing a PDMS stencil on a polystyrene culture dish (Falcon). The PDMS microstencil/polystyrene array was washed using ethanol and dried in the oven; finally, the surface of the PDMS stencil was treated with O_2 plasma in an asher.

The medium containing the cultured cells was poured over the PDMS microwell array or PDMS microstencil/polystyrene. After the cells were trapped in the microwells or the stencil, the surface was rinsed with a fresh medium to remove the additional cells, and the retained cells were cultured in the incubator at 37 °C under 5% CO_2 for 5–7 h. In the case of addition chemical stimulation to the cell, we continued the additional incubation of the cell array in the medium with chemicals (Shiku et al., 2009; Folch et al., 2000).

2.4. SECM analysis of the single-cell reporter assay

The single cells in the microwell array were further studied by scanning electrochemical microscopy (Fig. 1d). The single cells captured in the individual microwells of the array were washed with HEPES buffer (150 mM NaCl, 4.2 mM KCl, 2.7 mM $MgCl_2$, 1.0 mM Na_2HPO_4, 11.2 mM glucose, 10 mM HEPES, pH 7.0) and incubated in the same solution at 37 °C under 5% CO_2 atmosphere for 10 min. After incubation, the single-cell array was placed in 3 mL of a measuring solution containing 4.7 mM PAPP and HEPES buffer (pH 9.5). A two-electrode system comprising a Pt microdisk (diameter, 20 μm) as the working electrode and an Ag/AgCl reference/counter electrode was employed for the SECM measurements. The potential of the working electrode was set at 0.3 V vs. Ag/AgCl for facilitating the oxidation of PAP. An area of 600 μm × 450 μm or 600 μm × 600 μm was scanned by SCEM at a rate of 20 μm s^{-1} at room temperature. The pixel unit of the image was 10 μm × 10 μm. The height of the electrode tip in the constant-height mode SECM was set at 20 μm from the top of the SU-8 or PDMS microwells.

2.5. Live/dead fluorescence assay on single-cell arrays

The viability of the cells patterned on the stencil, under the conditions maintained during SECM measurements, was evaluated using a live/dead fluorescence kit (a combination of 2 fluorochromes, namely, calcein-AM and PI was used; Dojindo Laboratories, Japan). In the case of HeLa cells seeded in single-cell array with the PDMS microwell, almost all cells were alive (94%) for a period of 60 min after being soaked in the measuring solution (pH 9.5). It was also found that only 40% were alive for the single-cell array with the PDMS microwell, whereas more than 90% were alive for the cells patterned on a culture dish using a PDMS stencil of 300-μm diameter (Shiku et al., 2009), with the 120-min incubation in the measuring solution (pH 9.5) for 120 min at room temperature.

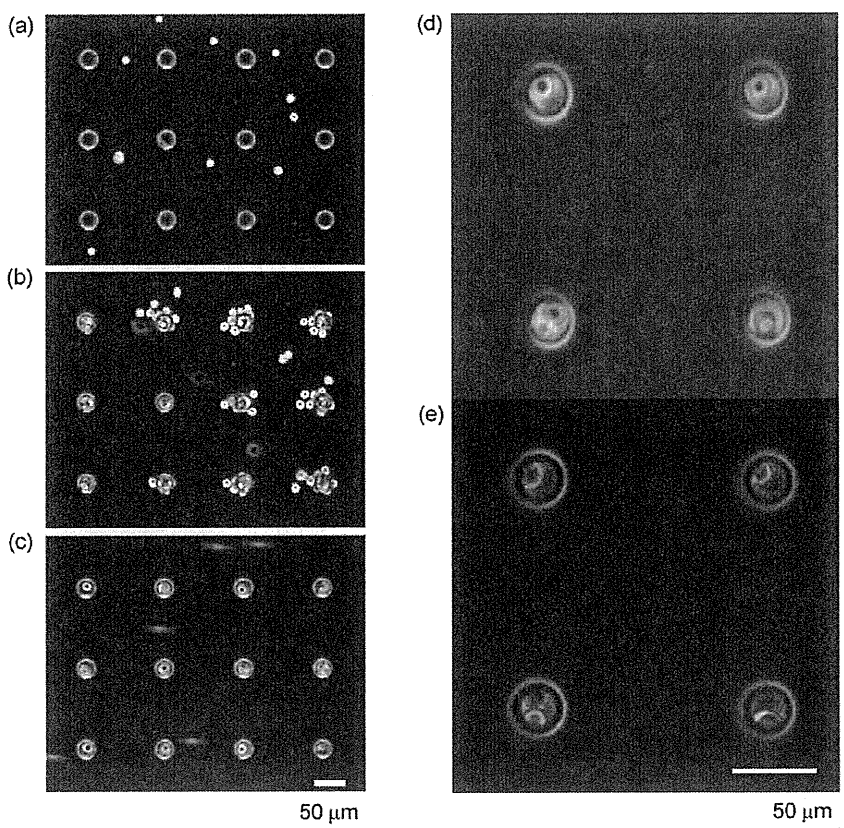

Fig. 2. (a–c) Sequential photographs acquired during the pDEP manipulation of cells on the SU-8 microwell array/ITO. (d) The single-cell array just after pDEP pulse application and the subsequent removal of the counter ITO electrode. (e) The cells after 5-h incubation in the culture medium. The diameter and depth of the microwells were 30 μm and 25 μm, respectively.

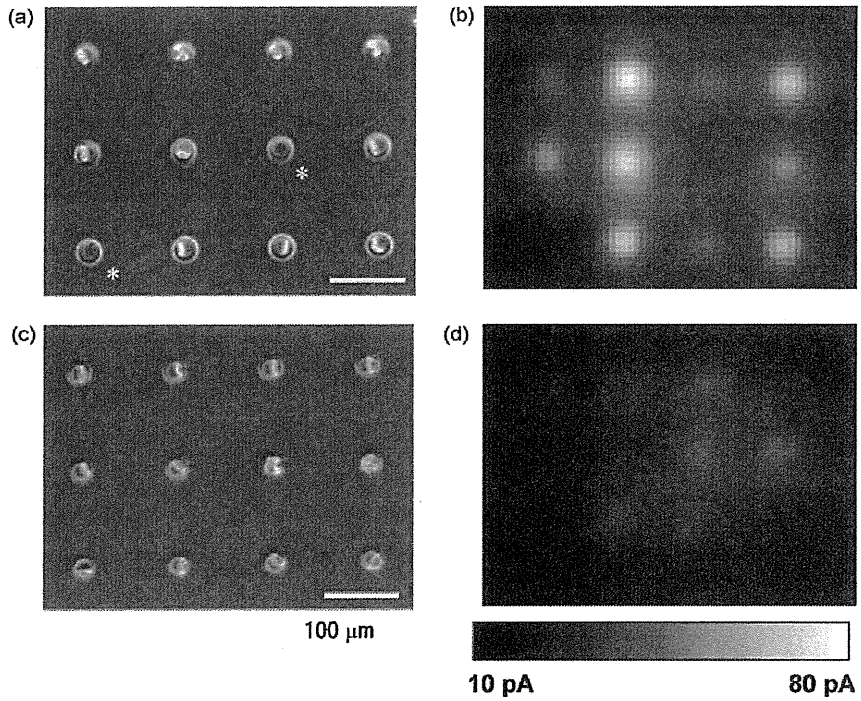

Fig. 3. Optical (a and c) and SECM images (b and d) of the single-cell array of HeLa-SEAP (a and b) and wild-type HeLa (c and d) cells on the SU-8 microwell array/ITO. SECM was performed in 4.7 mM PAPP, HEPES buffer (pH 9.5). The tip of the microelectrode (diameter, 20 μm) was used for scanning the cells from a 20 μm height and at a scan rate of 20 μm s^{-1}. The SECM scan area was 600 μm × 450 μm. The diameter and depth of the microwell were 30 and 25 μm, respectively. The vacant well was marked as (*).

3. Results and discussion

Fig. 2 shows the sequential photographs acquired during cell manipulation with pDEP. The cell suspension (density: 5×10^6–5×10^5 cells mL^{-1} of 0.2 M sucrose) was introduced into the flow-through device comprising the microwell array/ITO and a top ITO electrode, and an AC voltage (3 Vpp, 1 MHz) was applied between the 2 electrodes (Fig. 2a). The phase shift between the AC voltages applied to the 2 electrodes was set at 180° by using a pulse generator (Hioki E.E.). The surface of the well array/ITO was treated with O_2 plasma (Plasma asher, Yanaco). Within 10–20 s, the cells aggregated near the cylindrical microwell (Fig. 2b); subsequently, the AC voltage was turned off and the excess cells were removed by washing with a medium (Fig. 2c). The positive force generated during DEP was strong enough to retain the captured cell in the microwell even after the pulse was turned off. A simultaneous fluorescence viability assay indicated that the cells were alive and not damaged seriously as shown later. Fig. 2d shows a magnified view of the cells on the SU-8 microwell array/ITO just after pDEP manipulation; each microwell is observed to contain a single cell. Then, the top ITO electrode was removed and the single-cell array was soaked in culture medium and incubated for a further 5 h to promote active cellular adhesion to the electrode (Fig. 2e).

Next, the diameter and the height of the SU-8 wells were optimized. We constructed microwells with diameters of 20, 25, 30, 50, and 100 μm and depths of 10 and 25 μm. Fig. S-1 shows the arrays of cells formed by pDEP manipulation in the microwells with a depth of 25 μm and different diameters. Only a single cell was captured in microwells with diameter of 20 μm (Fig. S-1a) or 25 μm, as the diameter of the HeLa cell was ca. 20 μm. However, during washing, the entrapped cells were easily released from the wells. In addition, the cells tended to demonstrate apoptotic changes, since the well was too small for their survival (Chen et al., 1997; Nishizawa et al., 2002).

In microwells with a diameter of 30 μm, a single cell was captured because there was no room to accommodate another cell. As already shown in Fig. 2, application of the DEP pulse attracted many cells to the microwell; the excess cells were easily flushed out by a slow-flowing stream of the sucrose solution. After 5-h incubation in the culture medium, the cells were observed to adhere to the substrate, and the formation of lamellipodium was noted on the electrode (Fig. S-1b). Further, good cellular attachment on the electrode was also observed in the case of wells with a diameter of 50 μm, but an average of 3 cells were captured in these wells (Fig. S-1c). In the case of 100-μm diameter wells, the DEP force was effective at the edge of the electrode (Fig. S-2), and hence the cell number in these wells showed a broad distribution. Fig. S-1d shows the relation between the occupancy rate and the cell number in microwells of various sizes. The occupancy rate was defined as the percentage of the microwell occupied with a certain number of the cell (0–6 cells) out of the all microwells observed. The rates for single-cell occupancy were high in the case of microwells with diameters of 20 or 30 μm. Similar findings were noted for the microwells with a depth of 10 μm. However, the cells in the 10-μm deep microwells were easily flushed out by the washing or disassembling process (Chang et al., 2009). These results indicate that the single-cell array was most efficient when the microwells in the array chip had a diameter of 30 μm and a depth of 25 μm.

The viability of the cells in the microwell after pDEP was evaluated by using the live/dead fluorescence assay (Kaya et al., 2003; Torisawa et al., 2007). In order to determine the effects of the electric field and the dimensions of the microwell separately, we prepared 3 types of microwell arrays: microwell array/ITO, PDMS microwell array, and PDMS microstencil/polystyrene. We used the microwell array/ITO to evaluate the effect of the electric field; most of the entrapped single cells were alive (89.2%, $n = 137$), and this result was in accordance with those of a previous study (Gray et al., 2004). In the case of the PDMS microwell array and the PDMS microstencil/polystyrene, 100% and 98% of the entrapped cells were

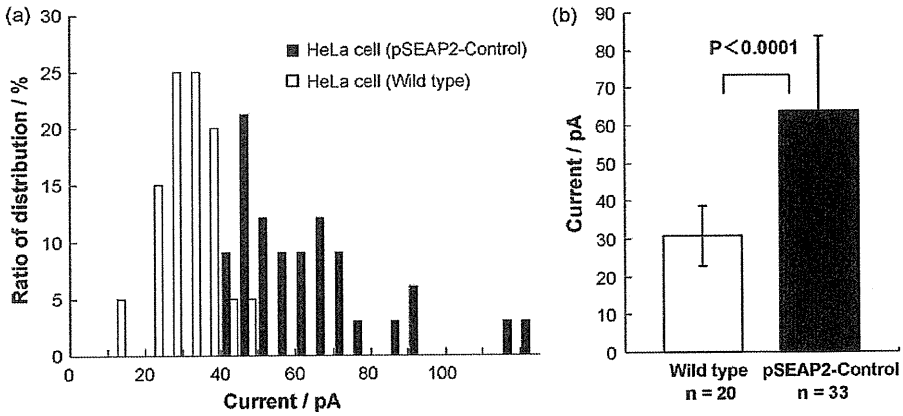

Fig. 4. (a) Histograms showing the ratio of distribution vs. the current response of HeLa-SEAP cells (filled bar) and wild-type HeLa cells (open bar) of the single-cell array on the SU-8 microwell array/ITO. (b) The average current response of HeLa-SEAP cells (filled bar, $n = 33$) and wild-type HeLa cells (open bar, $n = 30$). Error bar indicates the standard deviation.

alive, respectively. (See Supporting Information, Figs. S-3 and S-4.) The live/dead fluorescence assay revealed no significant difference between the viability of the cells among the 3 types of microwell arrays. However as shown later, this does not indicate that pDEP cellular manipulation is a stress-free technique against any cell line.

Next, we performed an electrochemical reporter assay on the single-cell array. HeLa cells (HeLa-SEAP) transfected with the plasmid vector (pSEAP2-control) containing the SEAP construct were selected for the reporter assay. The pSEAP2-control constitutively expressed the SEAP gene. The HeLa-SEAP and wild-type HeLa cells were independently localized on the 4 × 4 single-cell array device by pDEP manipulation. The cells were cultivated in culture medium for 5 h at 37 °C, and subsequently the device was soaked in 4.7 mM PAPP, HEPES buffer (pH 9.5). The cells remained alive for at least 1 h. A Pt electrode with 20-μm diameter was used for scanning the cells in the SU-8 microwell from a height of 20 μm at a scan rate of 20 μm s^{-1}. The potential of the tip of the Pt electrode was set at +0.3 V vs. Ag/AgCl. Fig. 3 shows the optical and SECM images of the single-cell array of HeLa-SEAP and wild-type HeLa cells suspended in 4.7 mM PAPP, HEPES buffer (pH 9.5). The diameter and depth of the SU-8 microwell were 30 μm and 25 μm, respectively. The PAP oxidation current responses were well corresponding to the position of the microwell. Although the planar design of the culture dish enabled single-cell SECM imaging for detecting the SEAP reporter activity of the cells, it was difficult to control the cell density of these cultures. For example, since the cells were at stages immediately after cell division, they were located very close to each other, which made it impossible to resolve the current response of the 2 newly formed cells. Moreover, elevation of the background response was also a problem because PAP was continuously produced by the hydrolysis of PAPP via SEAP catalysis. Fig. 4 shows the distributions of the current responses of single HeLa-SEAP and wild-type HeLa cells. The ratio of distribution was defined as the percentage of the single-cell sample with a certain range of the current responses out of the all the SECM measurements. The average ± standard deviation (SD) values for HeLa-SEAP and wild-type HeLa cells were 63.64 ± 20.06 (filled bar, $n = 33$) and 30.77 ± 7.88 pA (open bar, $n = 20$), respectively. The current response of the HeLa-SEAP cell was significantly larger than that of the non-transfected HeLa cell.

Single-cell SECM imaging and cell metabolism measurements have been already reported previously (Yasukawa et al., 1998; Kaya et al., 2003; Zhou et al., 2003; Bard et al., 2006; Schrock and Baur, 2007; Schulte and Schuhmann, 2007). Adherent cells show diverse distributions in the size, shape and cellular cycle phase. Therefore platform to arrange single-cell array becomes a useful

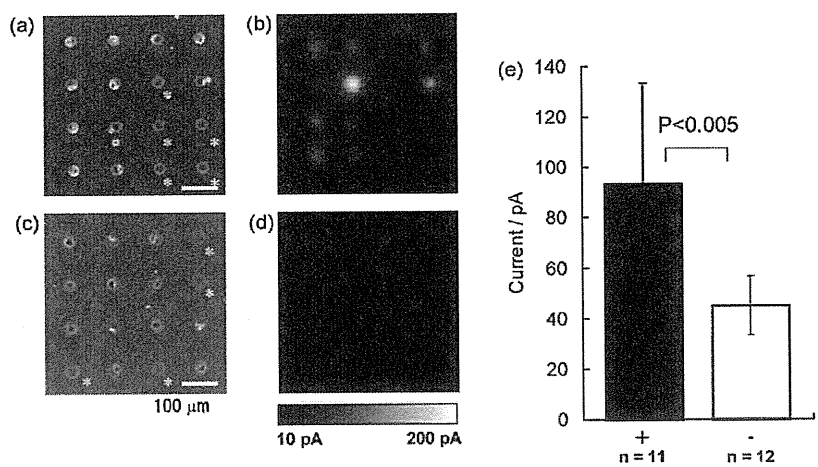

Fig. 5. The optical (a and c) and SECM images (b and d) of the single-cell array of HeLa-NFκB-SEAP cells with (a and b) and without (c and d) 100 ng mL^{-1} TNF-α stimulation on the PDMS stencil/polystyrene device not subjected to pDEP. The vacant well was marked as (*). SECM was performed in the same conditions as those mentioned in Fig. 4. The SECM scan area was 600 μm × 600 μm. (e) The average current response of the HeLa-NFκB-SEAP cells with (filled bar, $n = 11$) and without TNF-α stimulation (open bar, $n = 12$).

tool, especially for the purpose to monitor cellular signal transduction pathway. Microwell array is appropriate to control the diffusion of reactants and products from single cells because the concentration profile near the microwell is defined by the geometry of the microwell rather than the original shape and size of the cell entrapped (Shiku et al., 2004). We found that wild-type HeLa has endogenous (natural) alkaline phosphatase activity. Current response due to topographic change in the microwell may be negligible because we confirmed that there was no current response for the polystyrene beads without alkaline phosphatase on the SU-8 microwell array/ITO s shown in Fig. S-5.

As shown above, SECM allows statistic analysis of electrochemical responses from single cells. Therefore, we next tried to monitor the signal transduction in the cells by switching on/off the expression of the reporter gene that was under the control of promoter region, and which was responsible for the binding of the transcription factors at the responsive elements in the DNA sequences. We selected the NFκB pathway as the model, in which the NFκB protein complex binds to the κB element triggering transcription of the genes downstream of the promoter region. HeLa cells were transfected with a plasmid vector pNFκB-SEAP (HeLa-NFκB-SEAP) that secreted SEAP upon stimulation with TNF-α. Fig. 5 shows the optical and SECM images of the single-cell array of HeLa-NFκB-SEAP cells with and without TNF-α stimulation. The cells were arrayed in the PDMS microstencil/polystyrene without applying pDEP. Panels (a) and (b) were taken after the incubation with the RPMI medium for 5 h and with the RPMI medium containing 100 ng mL^{-1} TNF-α for 2 h. Panels (c) and (d) were taken after the incubation with the RPMI medium for 8 h. The average current response of HeLa-NFκB-SEAP (filled bar, $n=11$) cells stimulated with TNF-α was significantly larger than that of the untreated cells (open bar, $n=12$) (Fig. 5e), indicating that TNF-α activates the intracellular signaling pathway for the production of SEAP.

In order to clarify the influence of pDEP, the HeLa-NFκB-SEAP cells that localized on the SU-8 microwell array/ITO in the form of a 4×3 single-cell array after pDEP manipulation were subjected to SECM analysis. The SECM response in this case was very large even before stimulation with TNF-α. Moreover, this response was noted to increase during the 5-h culture, which promoted cell adhesion (Supplement, Fig S-6). This elevation of the background response was probably due to the stress by pDEP and/or the SU-8 material. Although almost all the cells were alive after DEP, it does not indicate that the pDEP manipulation is completely stress free. The SECM responses of the pDEP-manipulated single cells in the SU-8 microwell array/ITO were compared before and after TNF-α stimulation. The oxidation current responses of a single HeLa-NFκB-SEAP cell as determined by the single-scan mode SECM before and after TNF-α stimulation were 51.04 ± 14.42 ($n=7$) and 43.48 ± 7.87 pA ($n=8$), respectively. No significant difference was noted ($p > 0.25$).

In our previous studies, we have reported the use of a novel electrochemical device comprising orthogonally positioned arrays of column- and row-electrodes for the analysis of single-cell gene expression (Lin et al., 2009). By using the electrode array device, PAP produced from a single cell was oxidized at the row-electrode set at 0.3 V vs. Ag/AgCl. The oxidized product, i.e., *p*-quinoneimine (QI) underwent reduction to form PAP at the column electrode set at 0.0 V vs. Ag/AgCl; 100 points of the cross section of the column- and row-electrodes were collected within 22 s. However, typically, it takes 25 min to capture a single SECM image (600 μm × 450 μm, 12 microchambers). Although SECM imaging is not as fast as electrochemical analysis using our device previously reported, the oxidation current of ca. 60 pA obtained for a single HeLa-SEAP cell in the microchamber by using SECM was significantly larger than that obtained by using the electrochemical device (16.3 ± 5.49 pA ($n=67$)). This is because SECM estimates the PAP oxidation current from the upper side of the microwell with the simplest manner. The current response of several tens of pA obtained by SECM made the statistic analysis more reliable, and consequently, we were successful in accomplishing the electrochemical monitoring of the signal transduction pathways at the single-cell level for the first time.

4. Conclusion

In this study, the expression of SEAP was electrochemically monitored at the single-cell level by SECM. First, we constructed a single-cell array and subjected it to pDEP. The SECM response of HeLa cells that constitutively expressed SEAP (HeLa-pSEAP2-Control) was significantly large compared to that of the wild-type HeLa cells ($p < 0.0001$). Next, we transfected the HeLA cells with a plasmid containing SEAP under the control of a responsive element (κB element). The SECM measurements indicated that TNF-α stimulation remarkably increased the response of the transfected cells arrayed on the PDMS microstencil/polystyrene without subjecting them to pDEP. The average current responses of HeLa-NFκB-SEAP cells with and without TNF-α stimulation were significantly distinguishable ($p < 0.005$). However, a very high SECM response was obtained even before the stimulation of cells with TNF-α during single-cell manipulation by pDEP on the SU-8 microwell array/ITO. Moreover, the response of the untreated cells increased during the 5-h culture that promoted cell adhesion. These results suggest that the stress caused by pDEP and/or the SU-8 material triggers intracellular signaling to produce SEAP.

Acknowledgements

This work was partly supported by Grants-in-Aid for Scientific Research (18101006, 21685008) from MEXT (Ministry of Education, Culture, Sports, Science and Technology), Japan; by a Grant-in-Aid for Scientific Research on Priority Areas (17066002) "Life Surveyor" from MEXT; and by a grant from the Center for Interdisciplinary Research, Tohoku University.

Appendix A. Supplementary data

Supplementary data associated with this article can be found, in the online version, at doi:10.1016/j.bios.2009.09.001.

References

Bard, A.J., Fan, F.-R.F., Kwak, J., Lev, O., 1989. Anal. Chem. 61, 132–138.
Bard, A.J., Li, X., Zhan, W., 2006. Biosens. Bioelectron. 22, 461–472.
Chen, C.S., Mrksich, M., Huang, S., Whitesides, G.M., Ingber, D.E., 1997. Science 276, 425–1428.
Chang, C.-Y., Murata, T., Takahashi, Y., Shiku, H., Chang, H.-C., Matsue, T., 2009. Lab. Chip 9, 1185–1192.
Daunert, S., Barrett, G., Feliciano, J.S., Shetty, R.S., Shrestha, S., Spencer, W.S., 2000. Chem. Rev. 100, 2705–2738.
Di Carlo, D., Aghdam, N., Lee, L.P., 2006. Anal. Chem. 78, 4925–4930.
Folch, A., Jo, B.H., Hurtado, O., Beebe, D.J., Toner, M., 2000. J. Biomed. Mater. Res. 52, 346–353.
Gray, D.S., Tan, J.L., Voldman, J., Chen, C.S., 2004. Biosens. Bioelectron. 19, 771–780.
Hosokawa, M., Arakaki, A., Takahashi, M., Mori, T., Takeyama, H., Matsunaga, T., 2009. Anal. Chem. 81, 5308–5313.
Ino, K., Okochi, M., Konishi, N., Nakatochi, M., Imai, R., Shikida, M., Ito, A., Honda, A., 2008. Lab. Chip 8, 134–142.
Kaff, B.M., Voldman, J., 2005. Anal. Chem. 77, 7976–7983.
Kaya, T., Torisawa, Y.S., Oyamatsu, D., Nishizawa, M., Matsue, T., 2003. Biosens. Bioelectron. 18, 1379–1383.
Kelso, E., McLean, J., Cardosi, M.F., 2000. Electrocanalysis 12, 490–494.
Kovac, J.R., Voldman, J., 2007. Anal. Chem. 79, 9321–9330.
Kunikata, R., Takahashi, Y., Koide, M., Itayama, T., Yasukawa, T., Shiku, H., Matsue, T., 2009. Sens. Actuators B 141, 256–262.
Lee, H.J., Yasukawa, T., Suzuki, M., Taki, Y., Tanaka, A., Kameyama, M., Shiku, H., Matsue, T., 2008. Sens. Actuators B 131, 424–431.
Lee, H.J., Yasukawa, T., Suzuki, M., Lee, S.H., Yao, T., Taki, Y., Tanaka, A., Kameyama, M., Shiku, H., Matsue, T., 2009. Sens. Actuators B 136, 320–325, doi:10.1016/j.snb.2008.12.054.
Li, X., Bard, A.J., 2009. J. Electroanal. Chem. 628, 35–42.

Lin, Z., Takahashi, Y., Kitagawa, Y., Umemura, T., Shiku, H., Matsue, T., 2008. Anal. Chem. 80, 6830–6833.
Lin, Z., Takahashi, Y., Murata, T., Takeda, M., Ino, K., Shiku, H., Matsue, T., 2009. Angew. Chem. Int. Ed. 48, 2044–2046.
Matsue, T., Matsumoto, N., Koike, S., Uchida, I., 1993. Biochim. Biophys. Acta—Gen. Subjects 1157, 332–335.
Matsue, T., Matsumoto, N., Uchida, I., 1997. Electrochim. Acta 42, 3251–3256.
Matsumoto, N., Matsue, T., Uchida, I., 1994. Bioelectrochem. Bioenergy 34, 199–202.
Matsunaga, T., Hosokawa, M., Arakaki, A., Taguchi, T., Mori, T., Tanaka, T., Takeyama, H., 2008. Anal. Chem. 80, 5139–5145.
Mauzeroll, J., Bard, A.J., 2004. Proc. Natl. Acad. Sci. U.S.A. 101, 7862–7867.
Neugebauer, S., Zimdars, A., Liepold, P., Gebala, M., Schuhmann, W., Hartwich, G., 2009. Chem. Biol. Chem. 10, 1193–1199.
Nishizawa, M., Takoh, K., Matsue, T., 2002. Langmuir 18, 3645–3649.
Retting, J.R., Folch, A., 2005. Anal. Chem. 77, 5628–5634.
Roberts, W.S., Lonsdale, D.J., Griffiths, J., Higson, S.P.J., 2007. Biosens. Bioelectron. 23, 301–318.
Sasuga, Y., Iwasa, T., Terada, K., Oe, Y., Sorimachi, H., Ohara, O., Harada, Y., 2008. Anal. Chem. 80, 9141–9149.
Schrock, D.S., Baur, J.E., 2007. Anal. Chem. 79, 7053–7061.
Schulte, A., Schuhmann, W., 2007. Angew. Chem. Int. Ed. 46, 2–20.
Shiku, H., Takeda, M., Murata, T., Akiba, U., Hamada, F., Matsue, T., 2009. Anal. Chim. Acta 640, 87–92.
Shiku, H., Shiraishi, T., Aoyagi, S., Utsumi, Y., Matsudaira, M., Abe, H., Hoshi, H., Kasai, S., Ohya, H., Matsue, T., 2004. Anal. Chim. Acta 522, 51–58.
Sims, C.E., Allbritton, N.L., 2007. Lab. Chip 7, 423–440.
Skelley, A.M., Kirak, O., Suh, H., Jaenisch, R., Voldman, J., 2009. Nat. Methods 6, 147–152.
Suzuki, M., Yasukawa, T., Shiku, H., Matsue, T., 2008. Biosens. Bioelectron. 24, 1043–1047, doi:10.1016/j.bios.2008.06.051.
Takahashi, Y., Hirano, Y., Yasukawa, T., Shiku, H., Yamada, H., Matsue, T., 2006. Langmuir 22, 10299–10306.
Takahashi, Y., Miyamoto, T., Shiku, H., Asano, R., Yasukawa, T., Kumagai, I., Matsue, T., 2009. Anal. Chem. 81, 2785–2790.
Torisawa, Y.S., Ohara, N., Nagamine, K., Kasai, S., Yasukawa, T., Shiku, H., Matue, T., 2006. Anal. Chem. 78, 7625–7631.
Torisawa, Y.S., Takagi, A., Nashimoto, Y., Yasukawa, T., Shiku, H., Matsue, T., 2007. Biomaterials 28, 559–566.
Wittstock, G., Burchardt, M., Pust, S.E., Shen, Y., Zhao, C., 2007. Angew. Chem. Int. Ed. 46, 1584–1617.
Whitaker, R.D., Walt, D.R., 2007. Anal. Chem. 79, 9045–9053.
Yamamura, S., Kishi, H., Tokimitsu, Y., Kondo, S., Honda, R., Ramachandra Rao, S., Omori, M., Tamiya, E., Muraguchi, A., 2005. Anal. Chem. 77, 8050–8056.
Yasukawa, T., Kondo, Y., Uchida, I., Matasue, T., 1998. Chem. Lett. 27, 767–768.
Yasukawa, T., Nagamine, K., Horiguchi, Y., Shiku, H., Koide, M., Itayama, T., Shiraishi, F., Matsue, T., 2008. Anal. Chem. 80, 3722–3727.
Zhou, H., Kasai, S., Noda, H., Ohya-Nishiguchi, H., Shiku, H., Matsue, T., 2003. Bull. Chem. Soc. Jpn. 76, 1757–1762.

Human Reproduction, Vol.25, No.3 pp. 751–756, 2010
Advanced Access publication on January 18, 2010 doi:10.1093/humrep/dep455

human reproduction

ORIGINAL ARTICLE *Reproductive biology*

Progesterone decreases bone morphogenetic protein (BMP) 7 expression and BMP7 inhibits decidualization and proliferation in endometrial stromal cells

Ako Kodama, Osamu Yoshino, Yutaka Osuga[1], Miyuki Harada, Akiko Hasegawa, Kahori Hamasaki, Masashi Takamura, Kaori Koga, Yasushi Hirota, Tetsuya Hirata, Yuri Takemura, Tetsu Yano, and Yuji Taketani

Department of Obstetrics and Gynecology, Faculty of Medicine, University of Tokyo, 7-3-1, Hongo, Bunkyo-ku, Tokyo 113-8655, Japan

[1]Correspondence address. Tel: +81-3-3815-5411; Fax: +81-3-3816-2017; E-mail: yutakaos-tky@umin.ac.jp

BACKGROUND: Regulation of decidualization is decisive for proper implantation and the establishment of pregnancy. Recent studies have suggested that several bone morphogenetic proteins (BMPs) play physiological roles in reproduction. In the present study, we examined the expression of BMP7 in the endometrium and the effect of BMP7 on decidualization and proliferation of endometrial stromal cells (ESC).

METHODS: The gene expression of BMP7 in endometrial tissues collected from women with regular menstrual cycles was determined and the effect of ovarian steroid hormones on BMP7 gene expression was investigated in cultured ESC. The effect of BMP7 on the decidualization of ESC was determined by measuring the gene expression and protein secretion of insulin-like growth factor binding protein 1 (IGFBP1), a marker of decidualization. The effect of BMP7 on the proliferation of ESC was examined by the bromodeoxyuridine (BrdU) incorporation assay.

RESULTS: The gene expression of BMP7 in endometrial tissues was low at and after the mid-secretory phase of the menstrual cycle. Progesterone suppressed the gene expression of BMP7 in cultured ESC. Treatment with progesterone and estradiol for 12 days achieved decidualization of ESC, increasing the gene expression and protein secretion of IGFBP1. Addition of BMP7 protein to the culture almost completely inhibited these increases. BMP7 suppressed BrdU incorporation in ESC, which indicated an antiproliferative effect of BMP7 on ESC.

CONCLUSIONS: Progesterone-induced suppression of BMP7 and BMP7-induced inhibition of decidualization and proliferation of ESC suggest an elaborate regulatory mechanism for decidualization through BMP7 in the endometrium.

Key words: BMP7 / IGFBP1 / progesterone / decidualization / proliferation

Introduction

The endometrium undergoes dynamic changes during the menstrual cycle. Proper endometrial changes are essential for successful implantation, and aberrant endometrial status may lead to implantation failure. In addition to ovarian steroids, which have a central role in the regulation of morphological and functional changes to the endometrium, there are many local factors that modulate endometrial status (Kayisli *et al.*, 2004; Dimitriadis *et al.*, 2005).

Bone morphogenetic proteins (BMPs), together with growth differentiation factors (GDFs), comprise a subfamily of the transforming growth factor-β superfamily. BMPs and GDFs are multifunctional growth factors and their effects have been reported mainly in bone, cartilage, ligament and tendon formation (Francis-West *et al.*, 1999). However, BMPs and GDFs have also been demonstrated to control cellular proliferation, differentiation and apoptosis in reproductive tissues (Shimasaki *et al.*, 2004).

Gene expression of BMP2 (Ying and Zhao, 2000), BMP4 (Ying and Zhao, 2000), BMP6 (Lyons et al., 1989), BMP7 (Ozkaynak et al., 1997; Paria et al., 2001), GDF9 (Fitzpatrick et al., 1998) and GDF10 (Zhao et al., 1999) has been reported in the mouse uterus. These BMPs are expressed in a different spatiotemporal pattern and are thus speculated to have specific functions in the uterus. Mice deficient in ALK6, the receptor for these BMPs, have an abnormal endometrium and are infertile (Yi et al., 2001). A recent study has further demonstrated the presence of BMP2, BMP4, BMP7, GDF5, GDF8 and GDF11 in the human endometrium (Stoikos et al., 2008). BMP7 is unique among these BMPs in that its mRNA is lost from the uterine epithelium shortly after implantation in mice (Ozkaynak et al., 1997). In the human, gene expression of BMP7 has been reported in cultured endometrial stromal cells (ESC), with the expression level not being changed by cAMP-induced decidualization (Stoikos et al., 2008). In addition, immunostaining of human biopsied specimens have shown that BMP7 can be detected in highly decidualized cells with a vesicle staining pattern but not in first trimester deciduas (Stoikos et al., 2008).

Although these findings imply a functional role for BMP7 in endometrial physiology, to date there have been no studies examining the effects of BMP7 on the endometrium. To determine the possible roles of BMP7 in the human endometrium, in the present study, we first examined the gene expression of BMP7 in the endometrium. We then studied the effects of BMP7 on decidualization of ESC, measuring insulin-like growth factor binding protein 1 (IGFBP1) as a marker of decidualization (Harada et al., 2006). We also examined the effects of BMP7 on proliferation of ESC.

Materials and Methods

Patients and samples

Endometrial tissue was obtained from 39 women, either by curettage under sterile conditions or from women undergoing hysterectomy for benign gynecologic disease. The mean ($\pm$SD) age of the women was 37.8 $\pm$ 8.2 years. All women had regular menstrual cycles and none had received hormonal treatment within the 6 months prior to surgery. The specimens were dated according to the women's menstrual history. In order to avoid contamination with trophoblast cells, decidual tissues were collected from five women with ectopic pregnancy but without uterine bleeding, by dilation and curettage according to previous studies (Koga et al., 2001; Hirota et al., 2005). The experimental procedures were approved by the institutional review board of the University of Tokyo, and all women provided written informed consent for the use of their endometrial tissue.

Isolation and culture of human ESC

ESC were isolated and cultured as described previously (Koga et al., 2001; Yoshino et al., 2003). Fresh endometrial biopsy specimens collected in sterile medium were rinsed to remove blood cells. Tissues were minced into small pieces and incubated in DMEM/F-12 containing type I collagenase (0.25%; Sigma, St Louis, MO, USA) and deoxynuclease I (15 U/ml; Takara, Tokyo, Japan) for 60 min at 37°C. The resulting dispersed endometrial cells were separated by filtration through a 40-μm nylon cell strainer (Becton Dickinson, Franklin Lakes, NJ, USA). Any intact endometrial epithelial glands that remained were retained by the strainer, whereas dispersed ESC passed through the strainer into the filtrate. ESC in the filtrate were collected by centrifugation at 250*g* and resuspended in phenol red-free DMEM/F-12 containing 5% charcoal-stripped fetal bovine serum (FBS), 100 U/ml penicillin, 0.1 mg/ml streptomycin and 0.25 μg/ml amphotericin B. The ESC were seeded in a 100-mm culture plate and kept at 37°C in a humidified atmosphere of 5%CO_2–95% air. At the first passage, cells were plated at a density of 1×10^5 cells/ml into 12- or 96-well culture plates (Becton Dickinson) and used for further treatments.

Treatment of ESC

To determine the effects of estrogen and progesterone on the gene expression of BMP7 in ESC, ESC were treated with 2.5% charcoal/dextran-treated (stripped) FBS (HyClone, Logan, UT, USA) in the presence of estradiol (10 ng/ml) or progesterone (100 ng/ml) for 6, 12 and 24 h. To examine the effect of BMP7 on decidualization, *in vitro* decidualization was achieved as described previously (Koga et al., 2001). Briefly, after cells had reached 70% confluence in 12-well culture plates, they were rinsed and treated with 2.5% charcoal/dextran-treated (stripped) FBS in the presence of estradiol (10 ng/ml) plus progesterone (100 ng/ml) or 0.1% ethanol vehicle (control) for 12 days. BMP7 (0, 10 or 100 ng/ml; R&D Systems, Minneapolis, MN, USA) was also added to the culture medium. Culture media were collected and replenished every 3 days.

RNA extraction, reverse transcription and real-time quantitative PCR

Total RNA was extracted from endometrial tissues and ESC using an RNeasy Mini Kit (Qiagen, Hilden, Germany). After reverse transcription, real-time quantitative PCR and data analysis were performed using a LightCycler (Roche Diagnostic, Mannheim, Germany), as reported previously (Harada et al., 2006). Expression of BMP7 and IGFBP1 mRNA was normalized for RNA loading for each sample using human glyceraldehyde-3-phosphate dehydrogenase (GAPDH, Toyobo) mRNA as an internal standard. The BMP7 prrimers chosen (sense: 5′-GCCTACTACTGTGA GGGGGAG -3′; antisense: 5′-GAAGTAGAGGACGGAGATGGC-3′) amplified a 163-bp fragment. The IGFBP1 primers chosen (sense: 5′-GA GAGCACGGAGATAACTGAGG-3′; antisense: 5′-TTGGTGACATGGA GAGCCTTCG-3′) amplified a 131-bp fragment. The PCR conditions were as follows: for BMP7, 40 cycles of: 95°C for 10 s, 64°C for 10 s and 72°C for 4 s; for IGFBP1, 40 cycles of: 95°C for 10 s, 67°C for 10 s and 72°C for 5 s; for GAPDH, 30 cycles of: 95°C for 10 s, 64°C for 10 s, 72°C for 18 s. All PCR conditions were followed by melting curve analysis.

Measurement of IGFBP1 protein

Concentrations of IGFBP1 in the conditioned media were determined using a specific ELISA kit (R&D Systems, Minneapolis, MN, USA). The limit of sensitivity of the kit was 31.3 pg/ml. The concentrations measured were normalized against the total protein of cell lysates from each well of the culture plates.

5-Bromo-2′-deoxyuridine proliferation assay

The bromodeoxyuridine (BrdU) proliferation assay was performed as described previously (OuYang et al., 2008) using the Biotrak Cell Proliferation ELISA System (Amersham Biosciences, Piscataway, NJ, USA) according to the manufacturer's instructions. Briefly, after incubation of ESC in serum-free medium for 24 h in 96-well plates, cells were treated for a further 24 h with serum-free medium containing either BMP7 (0, 10, 100 ng/ml) or 20% charcoal-stripped FBS as a positive control. After the 24 h incubation, 100 μl BrdU solution was added and cells were incubated at 37°C for an additional 2 h.

Statistical analysis

Expression of BMP7 mRNA in endometrial tissues was analyzed by the Kruskal–Wallis test, whereas other data were analyzed by ANOVA. Both tests were followed by *post hoc* analysis for multiple comparisons. $P < 0.05$ was considered significant.

Results

Expression of BMP7 mRNA in endometrial tissue throughout the menstrual cycle and in progesterone- and estradiol-treated ESC

As shown in Fig. 1, expression of BMP7 mRNA in endometrial tissues was significantly lower in the mid- and late secretory phases and in the decidua compared with expression in the mid-proliferative phase. In cultured ESC, treatment with progesterone, but not estradiol, decreased BMP7 mRNA expression at 12 and 24 h, compared with 0 h, in a time-dependent manner (Fig. 2A). Long-term culture of ESC in the presence of progesterone and estradiol remarkably decreased BMP7 mRNA expression on Day 3 and later, and distinctly induced IGFBP1 mRNA expression on Day 12 (Fig. 2B).

Effect of BMP7 on gene expression and secretion of IGFBP1 from ESC

Treatment with estradiol and progesterone for 12 days induced IGFBP1 mRNA expression in ESC. However, the addition of 10 and 100 ng/ml BMP7 to the culture medium markedly decreased the expression of IGFBP1 mRNA induced by the hormonal treatment in ESC (Fig. 3A). Figure 3B shows secretion of IGFBP1 protein from ESC, which was induced by estradiol and progesterone treatment on Day 9 and was increased to higher levels on Day 12. The addition of BMP7 to the culture medium markedly reduced IGFBP1 protein secretion, to almost undetectable levels in the presence of 100 ng/ml BMP7.

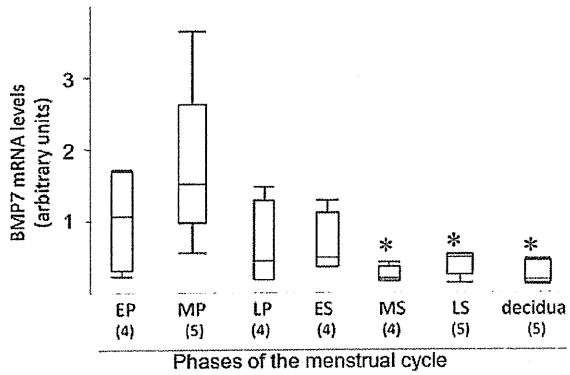

Figure 1 Expression of BMP7 mRNA in human endometrial tissues throughout the menstrual cycle and in early pregnant decidua.

Total RNA extracted from endometrial tissues and decidual tissues of ectopic pregnancies was reverse transcribed and then amplified by real-time PCR using primers for BMP7. Values were calculated by subtracting data for signal threshold cycles (Ct) of the internal standard (GAPDH) from Ct values for BMP7. The boxes represent the 25th and 75th percentiles. The median is denoted by the line that bisects the boxes. The whiskers indicate the extent of the data on the 1.5× interquartile range. *$P < 0.05$ compared with the MP. EP, early proliferative phase; MP, mid-proliferative phase; LP, late proliferative phase; ES, early secretory phase; MS, mid-secretory phase; LS, late secretory phase. The number of samples is shown in parentheses.

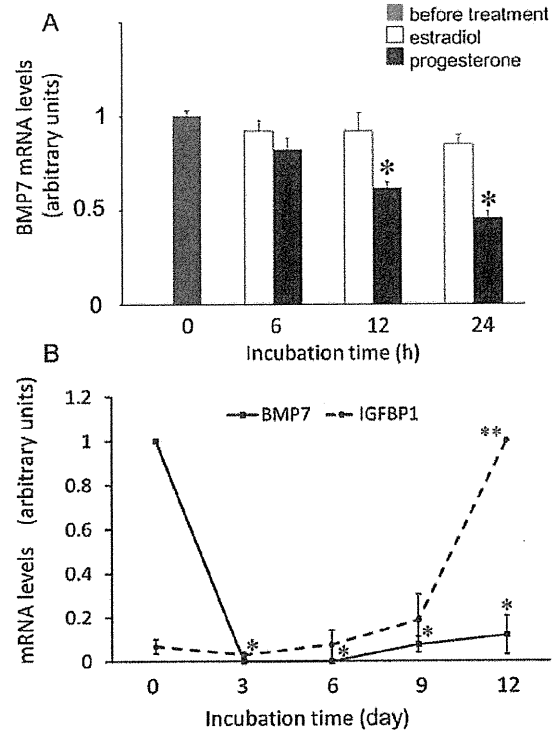

Figure 2 (**A**) Expression of BMP7 mRNA in ESC treated with estrogen (10 ng/ml) or progesterone (100 ng/ml) for 24 h. Data are the mean ± SEM of combined data from three independent experiments using different ESC from three patients. (**B**) Expression of BMP7 and IGFBP1 mRNA in ESC. *In vitro* decidualization of ESC was achieved by culturing ESC in the presence of estrogen (10 ng/ml) and progesterone (100 ng/ml) for 12 days. Data are the mean ± SEM of combined data from three independent experiments using different ESC from three patients. Total RNA isolated from ESC was reverse transcribed and then amplified by real-time PCR using primers for BMP7, IGFBP1 and GAPDH. Values were calculated by subtracting data for signal threshold cycles (Ct) of the internal standard (GAPDH) from Ct values for BMP7 or IGFBP1. (A) *$P < 0.05$ compared with 0 h. (B) *$P < 0.05$ compared with Day 0 (BMP7); **$P < 0.05$ compared with Day 0 (IGFBP1).

Effect of BMP7 on ESC proliferation

BMP7 at 10 and 100 ng/ml decreased BrdU incorporation in ESC by 20.5 ± 4.1 and 29.9 ± 4.2% (mean ± SEM of six replicate cultures) of the untreated controls, respectively (both $P < 0.05$ compared with the control), although 20% charcoal-stripped FBS increased BrdU incorporation by 134.8 ± 11.2%.

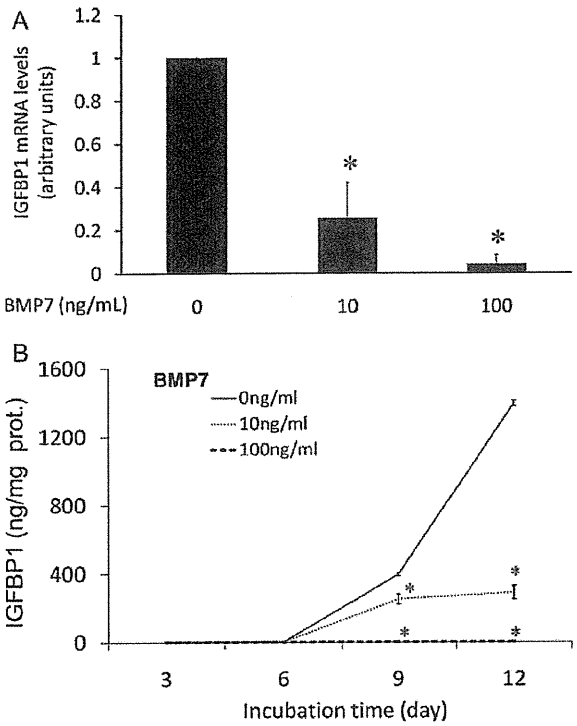

Figure 3 Effects of BMP7 on gene expression and protein secretion of IGFBP1 from ESC. (**A**) Effects of 10 and 100 ng/ml BMP7 on IGFBP1 mRNA expression in ESC treated with a combination of 10 ng/ml estradiol plus 100 ng/ml progesterone (EP) for 12 days. Total RNA isolated from ESC was reverse transcribed and then amplified by real-time PCR using primers for IGFBP1. Values were calculated by subtracting data for signal threshold cycles (Ct) of the internal standard (GAPDH) from Ct values for IGFBP1. Values are the mean ± SEM of four independent experiments using samples from four different patients. $^*P < 0.05$ versus 0 ng/ml. (**B**) IGFBP1 concentrations in culture media of ESC treated with EP, with or without BMP7 (10 and 100 ng/ml), for 3, 6, 9 and 12 days. IGFBP1 concentrations were determined using a specific ELISA and normalized against the total protein of cell lysates from each well. Data are the mean ± SEM of duplicate cultures. $^*P < 0.05$ compared with the respective control on each day. The result is representative of three separate experiments using samples from three different patients.

Discussion

In the present study, we demonstrated that gene expression of BMP7 in the endometrium was lower in the mid- and late secretory phases and in early pregnancy than in the mid-proliferative phase. Progesterone, but not estradiol, decreased BMP7 gene expression in ESC, which was significant after 12 h. Long-term incubation with progesterone and estradiol induced IGFBP1 protein secretion from ESC, which was inhibited by BMP7. BMP7 also decreased ESC proliferation.

In parallel with dynamic changes in the endometrium, the expression of many molecules in the endometrium changes spatiotemporally. Because embryos are accepted by the endometrium only during the 'implantation window', which corresponds to the mid-secretory phase, those substances for which levels in the endometrium change during the mid-secretory phase may have a role in preparing the receptive endometrium. In this context, the decrease in the gene expression of BMP7 in the mid-secretory phase may contribute to the development of the receptive endometrium.

Decidualization is a process in which remarkable structural and functional changes occur in ESC to prepare an appropriate environment for embryo implantation and maintenance of pregnancy. Decidualization is regulated by the ovarian steroid hormones estradiol and progesterone. In addition, the importance of other factors in the induction of decidualization has been demonstrated recently. For example, we found that mechanical stretch augments decidualization (Harada *et al.*, 2006), and others have found that paracrine factors are involved in decidualization (Tang *et al.*, 1994; Fazleabas and Strakova, 2002). The results of the present study, showing that BMP7 suppresses secretion of IGFBP1 protein from decidualizing ESC, suggest that BMP7 may act as an antidecidualization factor in the endometrium.

The antidecidualization activity of BMP7 is in marked contrast with the actions of BMP2, which increases the secretion of IGFBP1 and prolactin, another marker of decidualization, in decidualized ESC (Li *et al.*, 2007; Stoikos *et al.*, 2008). The expression patterns of BMP2 and BMP7 in the endometrium also appear to be different because *in-vitro* decidualization increases the expression of BMP2 in ESC (Li *et al.*, 2007). Thus, as a result of their different spatiotemporal expression, it is possible that the opposing actions of these two BMPs support decidualization and the subsequent establishment of pregnancy. From a therapeutic perspective, therapies targeted for BMP7 and BMP2 could be applicable for the treatment of implantation failure caused by impaired decidualization. Interestingly, the opposing functions of BMP7 and BMP2 have been demonstrated recently in adipogenesis, with BMP7 contributing to the development of brown adipocytes and BMP2 contributing to the development of white adipocytes (Tseng *et al.*, 2008).

The decrease in BMP7 expression in the decidualized endometrium may also be important for the successful development of the placenta. It has been shown that BMP7 suppresses the production of human chorionic gonadotrophin and progesterone from the trophoblast (Martinovic *et al.*, 1996). Because these hormones are tremendously important for the maintenance of pregnancy, the presence of BMP7 in the endometrium would be problematic for invading trophoblasts. Therefore, reduced BMP7 expression may be necessary not only for the development of a receptive endometrium, but also for the invading trophoblasts to establish pregnancy.

Progesterone inhibited BMP7 gene expression in ESC. This suggests that the decreased expression of BMP7 in the endometrium from the mid-secretory phase is due to the effects of progesterone. Notably, the inhibition of BMP7 gene expression by progesterone was clearly observed as early as 12 h. In addition, the decrease in BMP7 expression evidently preceded the increase in IGFBP1 expression during decidualization with progesterone and estradiol. This result, however, appears to be inconsistent with the findings by Stoikos *et al.* (2008) which showed that BMP7 gene expression was not altered by *in vitro* decidualization with cAMP . This difference may indicate that progesterone is prerequisite for down-regulation of BMP7 expression in the process of decidualization. Collectively,

progesterone may suppress BMP7 gene expression in the early stage to facilitate subsequent decidualization. Another apparently inconsistent finding of Stoikos *et al.* (2008) was the vesicular staining for BMP7 in decidual cells in mid–late secretory endometrium although staining patterns were not shown in other phases of the menstrual cycle. The decrease in BMP7 gene expression by progesterone might be involved in the change, if any, of intracellular localization of BMP7. Another possible explanation for the inconsistency may be any cross-reactivity of the antibody used in that study.

BMP7 appears to stimulate or inhibit proliferation depending on the cell type; for example, BMP7 stimulates proliferation of ovarian granulosa cells (Lee *et al.*, 2001) and Sertoli cells (Puglisi *et al.*, 2004), but inhibits proliferation of aortic smooth muscle cells (Dorai *et al.*, 2000), renal mesangial cells (Otani *et al.*, 2007) and prostate cancer cells (Miyazaki *et al.*, 2004). In the present study, BMP7 inhibited the proliferation of ESC. Thus, the decrease in BMP7 expression in the decidualized endometrium may contribute to the proliferation of decidual cells during pregnancy.

The present study has some limitations. First, the decidual tissues of ectopic pregnancies used in this study have advantages in that they are free from contamination with trophoblast cells, but they may have different characteristics from deciduas of normal pregnancies. Second, we measured mRNA levels but not protein levels of BMP7. Although cellular protein levels shown by immunostaining or immunoblotting are not necessarily proportional to their functional activities, knowledge about them would help our understanding of BMP7 in the endometrium. A further study is warranted regarding this point.

In summary, the results of the present study suggest that progesterone decreases BMP7 expression in the endometrium. The decrease in BMP7 expression may facilitate decidulalization of the endometrium, thus aiding the establishment of pregnancy.

Acknowledgements

The authors thank Emi Nose for her technical assistance.

Funding

This work was partially supported by Grants-in-Aid for Scientific Research from the Ministry of Education, Culture, Sports, Science and Technology and the Ministry of Health, Labour and Welfare.

References

Dimitriadis E, White CA, Jones RL, Salamonsen LA. Cytokines, chemokines and growth factors in endometrium related to implantation. *Hum Reprod Update* 2005;**11**:613–630.

Dorai H, Vukicevic S, Sampath TK. Bone morphogenetic protein-7 (osteogenic protein-1) inhibits smooth muscle cell proliferation and stimulates the expression of markers that are characteristic of SMC phenotype *in vitro*. *J Cell Physiol* 2000;**184**:37–45.

Fazleabas AT, Strakova Z. Endometrial function: cell specific changes in the uterine environment. *Mol Cell Endocrinol* 2002;**186**:143–147.

Fitzpatrick SL, Sindoni DM, Shughrue PJ, Lane MV, Merchenthaler IJ, Frail DE. Expression of growth differentiation factor-9 messenger ribonucleic acid in ovarian and nonovarian rodent and human tissues. *Endocrinology* 1998;**139**:2571–2578.

Francis-West PH, Parish J, Lee K, Archer CW. BMP/GDF-signalling interactions during synovial joint development. *Cell Tissue Res* 1999; **296**:111–119.

Harada M, Osuga Y, Takemura Y, Yoshino O, Koga K, Hirota Y, Hirata T, Morimoto C, Yano T, Taketani Y. Mechanical stretch upregulates IGFBP-1 secretion from decidualized endometrial stromal cells. *Am J Physiol Endocrinol Metab* 2006;**290**:E268–E272.

Hirota Y, Osuga Y, Hirata T, Koga K, Yoshino O, Harada M, Morimoto C, Nose E, Yano T, Tsutsumi O *et al.* Evidence for the presence of protease-activated receptor 2 and its possible implication in remodeling of human endometrium. *J Clin Endocrinol Metab* 2005;**90**:1662–1669.

Kayisli UA, Guzeloglu-Kayisli O, Arici A. Endocrine-immune interactions in human endometrium. *Ann N Y Acad Sci* 2004;**1034**:50–63.

Koga K, Osuga Y, Tsutsumi O, Yano T, Yoshino O, Takai Y, Matsumi H, Hiroi H, Kugu K, Momoeda M *et al.* Demonstration of angiogenin in human endometrium and its enhanced expression in endometrial tissues in the secretory phase and the decidua. *J Clin Endocrinol Metab* 2001;**86**:5609–5614.

Lee WS, Otsuka F, Moore RK, Shimasaki S. Effect of bone morphogenetic protein-7 on folliculogenesis and ovulation in the rat. *Biol Reprod* 2001; **65**:994–999.

Li Q, Kannan A, Wang W, Demayo FJ, Taylor RN, Bagchi MK, Bagchi IC. Bone morphogenetic protein 2 functions via a conserved signaling pathway involving Wnt4 to regulate uterine decidualization in the mouse and the human. *J Biol Chem* 2007;**282**:31725–31732.

Lyons K, Graycar JL, Lee A, Hashmi S, Lindquist PB, Chen EY, Hogan BL, Derynck R. Vgr-1, a mammalian gene related to Xenopus Vg-1, is a member of the transforming growth factor beta gene superfamily. *Proc Natl Acad Sci USA* 1989;**86**:4554–4558.

Martinovic S, Latin V, Suchanek E, Stavljenic-Rukavina A, Sampath KI, Vukicevic S. Osteogenic protein-1 is produced by human fetal trophoblasts *in vivo* and regulates the synthesis of chorionic gonadotropin and progesterone by trophoblasts *in vitro*. *Eur J Clin Chem Clin Biochem* 1996;**34**:103–109.

Miyazaki H, Watabe T, Kitamura T, Miyazono K. BMP signals inhibit proliferation and *in vivo* tumor growth of androgen-insensitive prostate carcinoma cells. *Oncogene* 2004;**23**:9326–9335.

Otani H, Otsuka F, Inagaki K, Takeda M, Miyoshi T, Suzuki J, Mukai T, Ogura T, Makino H. Antagonistic effects of bone morphogenetic protein-4 and -7 on renal mesangial cell proliferation induced by aldosterone through MAPK activation. *Am J Physiol Renal Physiol* 2007; **292**:F1513–F1525.

OuYang Z, Hirota Y, Osuga Y, Hamasaki K, Hasegawa A, Tajima T, Hirata T, Koga K, Yoshino O, Harada M *et al.* Interleukin-4 stimulates proliferation of endometriotic stromal cells. *Am J Pathol* 2008;**173**:463–469.

Ozkaynak E, Jin DF, Jelic M, Vukicevic S, Oppermann H. Osteogenic protein-1 mRNA in the uterine endometrium. *Biochem Biophys Res Commun* 1997;**234**:242–246.

Paria BC, Ma W, Tan J, Raja S, Das SK, Dey SK, Hogan BL. Cellular and molecular responses of the uterus to embryo implantation can be elicited by locally applied growth factors. *Proc Natl Acad Sci USA* 2001; **98**:1047–1052.

Puglisi R, Montanari M, Chiarella P, Stefanini M, Boitani C. Regulatory role of BMP2 and BMP7 in spermatogonia and Sertoli cell proliferation in the immature mouse. *Eur J Endocrinol* 2004;**151**:511–520.

Shimasaki S, Moore RK, Otsuka F, Erickson GF. The bone morphogenetic protein system in mammalian reproduction. *Endocr Rev* 2004;**25**:72–101.

Stoikos CJ, Harrison CA, Salamonsen LA, Dimitriadis E. A distinct cohort of the TGFbeta superfamily members expressed in human endometrium regulate decidualization. *Hum Reprod* 2008;**23**:1447–1456.

Tang B, Guller S, Gurpide E. Mechanism of human endometrial stromal cells decidualization. *Ann N Y Acad Sci* 1994;**734**:19–25.

Tseng YH, Kokkotou E, Schulz TJ, Huang TL, Winnay JN, Taniguchi CM, Tran TT, Suzuki R, Espinoza DO, Yamamoto Y *et al.* New role of bone morphogenetic protein 7 in brown adipogenesis and energy expenditure. *Nature* 2008;**454**:1000–1004.

Yi SE, LaPolt PS, Yoon BS, Chen JY, Lu JK, Lyons KM. The type I BMP receptor BmprIB is essential for female reproductive function. *Proc Natl Acad Sci USA* 2001;**98**:7994–7999.

Ying Y, Zhao GQ. Detection of multiple bone morphogenetic protein messenger ribonucleic acids and their signal transducer, Smad1, during mouse decidualization. *Biol Reprod* 2000;**63**:1781–1786.

Yoshino O, Osuga Y, Hirota Y, Koga K, Hirata T, Yano T, Ayabe T, Tsutsumi O, Taketani Y. Endometrial stromal cells undergoing decidualization down-regulate their properties to produce proinflammatory cytokines in response to interleukin-1 beta via reduced p38 mitogen-activated protein kinase phosphorylation. *J Clin Endocrinol Metab* 2003;**88**:2236–2241.

Zhao R, Lawler AM, Lee SJ. Characterization of GDF-10 expression patterns and null mice. *Dev Biol* 1999;**212**:68–79.

Submitted on July 2, 2009; resubmitted on December 2, 2009; accepted on December 4, 2009